



# Intercomparison of the comparative reactivity method (CRM) and pump–probe technique for measuring total OH reactivity in an urban environment

R. F. Hansen<sup>1,3,a</sup>, M. Blocquet<sup>4</sup>, C. Schoemaeker<sup>4</sup>, T. Léonardis<sup>1,2</sup>, N. Locoge<sup>1,2</sup>, C. Fittschen<sup>4</sup>, B. Hanoune<sup>4</sup>, P. S. Stevens<sup>3,5</sup>, V. Sinha<sup>6</sup>, and S. Dusanter<sup>1,2,4</sup>

<sup>1</sup>Mines Douai, SAGE, 59508 Douai, France

<sup>2</sup>Université de Lille, Lille, France

<sup>3</sup>Department of Chemistry, Indiana University, Bloomington, IN, USA

<sup>4</sup>Université de Lille, PhysicoChimie des Processus de Combustion et de l'Atmosphère (PC2A) UMR 8522 CNRS/Lille 1, Cité scientifique, 59655 Villeneuve d'Ascq Cedex, France

<sup>5</sup>School of Public and Environmental Affairs, Indiana University, Bloomington, IN, USA

<sup>6</sup>Department of Earth and Environmental Sciences, Indian Institute of Science Education and Research Mohali, Sector 81, S. A. S. Nagar, Manauli PO, Punjab 140306, India

<sup>a</sup>now at: School of Chemistry, University of Leeds, Leeds, LS2 9JT, UK

Correspondence to: R. F. Hansen (r.f.hansen@leeds.ac.uk)

**Abstract.** The investigation of hydroxyl radical (OH) chemistry during intensive field campaigns has led to the development of several techniques dedicated to ambient measurements of total OH reactivity, which is the inverse of the OH lifetime. Three techniques are currently used during field campaigns, including the total OH loss rate method, the pump–probe method, and the comparative reactivity method. However, no formal intercomparison of these techniques has been published so far, and there is a need to ensure that measurements of total OH reactivity are consistent among the different techniques.

An intercomparison of two OH reactivity instruments, one based on the comparative reactivity method (CRM) and the other based on the pump–probe method, was performed in October 2012 in a NO<sub>x</sub>-rich environment, which is known to be challenging for the CRM technique. This study presents an extensive description of the two instruments, the CRM instrument from Mines Douai (MD-CRM) and the pump–probe instrument from the University of Lille (UL-FAGE), and highlights instrumental issues associated with the two techniques.

It was found that the CRM instrument used in this study underestimates ambient OH reactivity by approximately 20 % due to the photolysis of volatile organic compounds (VOCs) inside the sampling reactor; this value is dependent

on the position of the lamp within the reactor. However, this issue can easily be fixed, and the photolysis of VOCs was successfully reduced to a negligible level after this intercomparison campaign. The UL-FAGE instrument may also underestimate ambient OH reactivity due to the difficulty to accurately measure the instrumental zero. It was found that the measurements are likely biased by approximately 2 s<sup>-1</sup>, due to impurities in humid zero air.

Two weeks of ambient sampling indicate that the measurements performed by the two OH reactivity instruments are in agreement, within the measurement uncertainties for each instrument, for NO<sub>x</sub> mixing ratios up to 100 ppbv. The CRM technique has hitherto mainly been used in low-NO<sub>x</sub> environments, i.e. environments with ambient NO<sub>x</sub> mixing ratios lower than a few ppbv, due to a measurement artifact generated by ambient NO inside the sampling reactor. However, this study shows that this technique can also be used under NO<sub>x</sub>-rich conditions if a NO<sub>x</sub>-dependent correction is carefully applied on the OH reactivity measurements.

A full suite of 52 VOCs, NO<sub>x</sub>, and other inorganic species were monitored during this intercomparison. An investigation of the OH reactivity budget for this urban site suggests that this suite of trace gases can account for the measured total OH reactivity.

## 1 Introduction

A detailed understanding of atmospheric oxidation processes is key to tackling fundamental issues related to air quality and climate change. For instance, the oxidation of volatile organic compounds (VOCs) in the presence of  $\text{NO}_x$  leads to the formation of photochemical pollutants such as ozone and secondary organic aerosols, which can have detrimental effects on both human health (Gryparis et al., 2004) and ecosystems (Ashmore, 2005). In addition, the lifetime of climate-related trace gases such as methane (Ehhalt, 1998) is mainly controlled by the atmospheric oxidative capacity; thus, the reliability of climate projections will strongly depend on the ability of models to correctly describe atmospheric oxidation processes.

While several free radicals initiate the oxidation of trace gases, the hydroxyl radical (OH) is the dominant oxidant in the daytime troposphere. It is therefore important to ensure that the initiation, propagation, and termination processes of OH are well understood and well-described in current atmospheric chemical models.

The loss of OH due to a reactive chemical species X can be quantified by the OH reactivity ( $k_X$ ), which is defined as the product of the appropriate rate constant for the reaction of X with OH ( $k_{X,\text{OH}}$ ) and the concentration of X, as shown in Eq. (1). The total OH reactivity ( $k_{\text{OH}}$ ) can be calculated by summing  $k_X$  for each chemical species  $X_i$  that reacts with OH in ambient air (Eq. 2).

$$k_X = k_{X,\text{OH}}[X], \quad (1)$$

$$k_{\text{OH}} = \sum_i k_{X_i,\text{OH}}[X_i] \quad (2)$$

Total OH reactivity ( $k_{\text{OH}}$ ) is a useful metric to test our understanding of OH chemistry, since it represents the total first-order loss rate of OH, i.e. the inverse of its lifetime. Indeed, total OH reactivity has been widely used in combination with OH and VOC concentration measurements to investigate the budget of OH sources and sinks as discussed below.

To determine the contribution of identified OH sinks to the total loss rate of OH, the OH reactivity calculated from trace gas measurements (Eqs. 1, 2) is compared to the measured total OH reactivity. Any discrepancy between measured and calculated total OH reactivity values represents OH sinks that have not been characterized by trace gas measurements and indicates that potentially important unmeasured reactive species and chemical processes associated with these species may impact our understanding of OH chemistry. Summaries of OH reactivity measurements performed during field campaigns (e.g., Table 1 in this work and Table 1 in Lou et al., 2010) show that discrepancies between measured and calculated OH reactivity have indeed been seen in a variety of environments. For example, two field campaigns, one conducted in a boreal forest (Nölscher et al., 2012a) and one conducted in a European megacity (Dolgorouky et al., 2012), have shown that the missing OH reactivity could represent

more than 50 % of the total OH reactivity. These studies highlight that our understanding of OH sinks is still incomplete.

Concomitant measurements of OH concentrations and OH reactivity can also be used to investigate the completeness of OH sources. Based on the assumption that the concentration of OH is in steady state, due to its short lifetime ( $< 1$  s), the total OH loss rate calculated from the measured  $k_{\text{OH}}$  and OH concentrations ( $k_{\text{OH}} \times [\text{OH}]$ ) can be compared to OH production rates calculated from known OH production pathways such as  $\text{O}_3+h\nu$ ,  $\text{HONO}+h\nu$ , and  $\text{HO}_2+\text{NO}$ , using measurements of trace gases and photolysis frequencies. Only a few studies have employed this approach, as collocated measurements of OH and OH reactivity, both made by complex instruments, are needed. Two of these studies, which compared OH production and loss rates for Beijing (Lu et al., 2013) and the Pearl River Delta (Hofzumahaus et al., 2009; Lu et al., 2012), found that OH production rates calculated from OH precursors were lower than the measured OH loss rates in both locations. These results suggest that there are still unknown sources of OH in these environments.

Total OH reactivity can also be used to examine ozone formation by determining if an air mass is  $\text{NO}_x$ - or VOC-limited with respect to ozone production (Kirchner et al., 2001). This can be used to determine ozone production regimes on local and regional scales and to calculate instantaneous ozone production rates as shown for the DOMINO field campaign (Sinha et al., 2012). More recently, Kumar and Sinha (2014) have shown that CRM coupled to sequential ambient VOC measurements using a new “VOC-OHM” system can be used to constrain the rate coefficient of the reactive nominal isobaric compound contributing to a given  $m/z$  ratio (e.g. isoprene and furan at  $m/z = 69$ ), adding more specificity to mass spectrometers with unity mass resolution.

Three techniques have been proposed in the literature to measure total OH reactivity: the total OH loss rate method (TOHLM) (Kovacs and Brune, 2001), the pump–probe method (Sadanaga et al., 2004b), and the comparative reactivity method (CRM) (Sinha et al., 2008b). As shown in Tables 1 and 2, all three techniques have been developed in different laboratories (Table 2) and total OH reactivity has been measured in several field campaigns encompassing a wide variety of environments (Table 1). The summary of ambient OH reactivity measurements, presented as Table 1, indicates that measurements of OH reactivity are now an established component of many atmospheric field campaigns.

The total OH loss rate method (Kovacs and Brune, 2001) was the first approach developed for OH reactivity measurements; this method uses a flow tube reactor to monitor OH kinetics in a flow of ambient air. OH radicals are generated in a movable injector located within the reactor by the photolysis of water vapor at 184.9 nm, leading to the production of both OH and  $\text{HO}_2$  radicals. The injector is moved within the reactor to record time-resolved OH decays with a resolution of 2.5–4 min (Table 2). A fraction of the flow at the output of the reactor (approximately  $10 \text{ L min}^{-1}$ ) is sampled

**Table 1.** Listing of previous OH reactivity field measurement campaigns (updated from Lou et al., 2010 and Hansen et al., 2014).

Campaign	Site	Dates	Environment	Technique	Collocated measurements <sup>a</sup>	MR <sup>b</sup>	Reference
SOS	Nashville, TN, USA	Jun–Jul 1999	Urban	TOHLM	HICOF	1.4	Kovacs et al. (2003)
PROPHET 2000	Michigan, USA	Jul–Aug 2000	Forest (mixed)	TOHLM	HIC <sup>c</sup>	~ 1.5	Di Carlo et al. (2004)
TexAQS2000	Houston, TX, USA	Aug–Sep 2000	Urban	TOHLM	HICOFB <sup>d</sup>	~ 1	Mao et al. (2010)
PMTACS-NY	New York City, USA	Jun–Aug 2001	Megacity	TOHLM	HICOF	~ 1	Ren et al. (2003)
–	Pennsylvania, USA	May–Jun 2002	Rural	TOHLM	HI <sup>e</sup>	–	Ren et al. (2005)
PMTACS	Whiteface Mountain, NY, USA	Jul–Aug 2002	Forest (mixed)	TOHLM	HICOF	~ 1	Ren et al. (2006b)
MCMA 2003/MILAGRO	Mexico City, Mexico	Apr 2003	Megacity	TOHLM	HICF <sup>e</sup>	–	Shirley et al. (2006)
–	Tokyo, Japan	Jul–Aug 2003	Megacity	Pump–probe	ICOFB	1.4–1.5	Sadanaga et al. (2004a)
PMTACS	New York City, USA	Jan–Feb 2004	Megacity	TOHLM	HICF	< 1.5	Ren et al. (2006a)
TORCH-2	Weybourne, Norfolk, UK	May 2004	Coastal marine	TOHLM	HICOF	1.6	Lee et al. (2009)
–	Tokyo, Japan	Nov 2004	Megacity	Pump–probe	ICOFB	1.3	Yoshino et al. (2006)
–	Mainz, Germany	Aug 2005	Urban	CRM	–	–	Sinha et al. (2008b)
–	Brownsberg, Suriname	Oct 2005	Forest (tropical)	CRM	CO	~ 3.5	Sinha et al. (2008b)
INTEX-B	Pacific Ocean	Apr–May 2006	Marine	TOHLM	HICOF	2.5	Mao et al. (2009)
PRIDE-PRD2006	Pearl River Delta, China	Jul 2006	Rural	Pump–probe	HIC	~ 2	Lou et al. (2010)
TRAMP2006	Houston, TX, USA	Aug–Sep 2006	Urban	TOHLM	HICOFB	~ 1	Mao et al. (2010)
–	Tokyo, Japan	Aug 2007	Megacity	Pump–probe	ICOFB	~ 1.4	Chatani et al. (2009)
OP-3	Borneo, Malaysia	Apr–May 2008	Forest (tropical)	TOHLM	HICOFB <sup>f</sup>	~ 2	Edwards et al. (2013)
SMEAR-BFORM	Hyytiälä, Finland	Aug 2008	Forest (boreal)	CRM	ICOB	~ 2	Sinha et al. (2010)
BEACHON-SRM08	Colorado, USA	Aug 2008	Forest (conifer)	Pump–probe	ICOB	1.4	Nakashima et al. (2014)
DOMINO	El Arenosillo, Spain	Nov–Dec 2008	Coastal marine	CRM	HIF <sup>e</sup>	–	Sinha et al. (2012)
BEARPEX09	California, USA	Jun–Jul 2009	Forest (conifer)	TOHLM	HICOFB	~ 1.5	Mao et al. (2012)
CABINEX <sup>g</sup>	Michigan, USA	Jul–Aug 2009	Forest (mixed)	CRM	COB	~ 1	Kim et al. (2011)
CABINEX <sup>h</sup>	Michigan, USA	Jul–Aug 2009	Forest (mixed)	TOHLM	HICOFB	~ 2	Hansen et al. (2014)
MEGAPOLI	Paris, France	Jan–Feb 2010	Megacity	CRM	ICO	~ 2	Dolgorouky et al. (2012)
CalNex-SJV	California, USA	May–Jun 2010	Rural	TOHLM	HICO	–	Pusede et al. (2014)
HUMPPA-COPEC	Hyytiälä, Finland	Jul–Aug 2010	Forest (boreal)	CRM	ICOFB	3–9	Nölscher et al. (2012a)
–	Lille, France	Oct 2012	Urban	CRM, FAGE	ICOF <sup>i</sup>	~ 1	This work

<sup>a</sup> Measurements made at the same location. Key: H = HO<sub>x</sub>, I = inorganics (including CO), C = anthropogenic NMHCs (including isoprene), O = OVOCs (excluding formaldehyde), F = formaldehyde, B = biogenic VOCs (BVOCs). <sup>b</sup> Missing OH reactivity fraction, expressed as a ratio of measured OH reactivity to calculated OH reactivity (Lou et al., 2010). <sup>c</sup> OVOCs, Formaldehyde, and BVOCs estimated from 1998 PROPHET campaign for OH reactivity calculation. <sup>d</sup> Based on description from Mao et al. (2010). <sup>e</sup> Measurements not used to calculate OH reactivity for this campaign. <sup>f</sup> Measurements of isoprene oxidation products not used in OH reactivity calculations. <sup>g</sup> Branch enclosure measurements. <sup>h</sup> Ambient measurements. <sup>i</sup> No measurements of CO, limited coverage of measurements for OVOCs, formaldehyde.

**Table 2.** Summary of OH reactivity instruments.

Technique	Reference	LOD (s <sup>-1</sup> ) <sup>a</sup> time res. (min)	Institution	Comments
Total OH loss rate method (TOHLM)	Kovacs and Brune (2001)	2.4/4	Penn State University (USA)	Laminar-flow reactor
	Ingham et al. (2009)	2.0/5	University of Leeds (UK)	Turbulent-flow reactor
	Hansen et al. (2014)	2.1/2.5	Indiana University (USA)	Turbulent-flow reactor
Pump–probe	Sadanaga et al. (2004b)	– <sup>b</sup> / 3 <sup>c</sup>	Tokyo Metropolitan University (Japan)	–
	Lou et al. (2010)	0.9 <sup>d</sup> / 1–3	Forschungszentrum Jülich (Germany)	–
	This work, Parker et al. (2011)	3.6–0.9 / 1–3	Université Lille – PC2A (France)	–
	Stone et al. (2015)	1–1.5 / 1–3	University of Leeds (UK)	–
Comparative reactivity method (CRM)	Sinha et al. (2008b)	3.5–6 <sup>e</sup> / 1	Max Planck Institute Mainz (Germany)	PTR-QMS <sup>f</sup> for pyrrole meas.
	Kim et al. (2011)	15 / – <sup>b</sup>	NCAR (USA)	PTR-QMS Branch enclosure meas.
	Nölscher et al. (2012b) <sup>g</sup>	3–6 <sup>h</sup> / 1	Max Planck Institute Mainz (Germany)	GC-PID for pyrrole meas.
	Dolgorouky et al. (2012)	3.0/2 <sup>i</sup>	LSCE (France)	PTR-QMS
	Kumar and Sinha (2014)	4/1	IISER Mohali (India)	PTR-QMS
This work	3.4/5	Mines Douai (France)	PTR-ToFMS	

<sup>a</sup> Limit of detection: 3σ unless otherwise stated; <sup>b</sup> value not reported; <sup>c</sup> value reported by Yoshino et al. (2006); <sup>d</sup> LOD determined from 3σ on zero-air decays reported by Lou et al. (2010); <sup>e</sup> LOD of 6 s<sup>-1</sup> reported by Sinha et al. (2008b), LOD of 3.5 s<sup>-1</sup> reported by Sinha et al. (2010); <sup>f</sup> Proton Transfer Reaction-Quadrupole Mass Spectrometry; <sup>g</sup> all values taken from Table 2 of this reference; <sup>h</sup> value reported for 2σ, relative to C<sub>2</sub>; <sup>i</sup> based on frequency measurements reported in Fig. 8 of this reference.

into an OH detection cell employing the Fluorescence Assay with Gas Expansion (FAGE) technique (Faloona et al., 2004; Dusanter et al., 2009).

A laminar-flow version of this instrument requires a sample flow rate of approximately 60–100 L min<sup>-1</sup> (Kovacs and Brune, 2001), whereas turbulent-flow instruments require

sample flow rates on the order of 100–400 L min<sup>-1</sup> to establish turbulent conditions within the reactor (Ingham et al., 2009; Hansen et al., 2014). The TOHLM technique is susceptible to measurement artifacts from ambient NO due to the formation of OH inside the sampling reactor from the HO<sub>2</sub>+NO reaction. However, a correction procedure has been developed (Ren et al., 2003; Shirley et al., 2006), using simultaneous measurements of ambient NO and HO<sub>2</sub> within the reactor. TOHLM instruments have relatively low limits of detection (1–2 s<sup>-1</sup>; see Table 2), and total OH reactivity values up to 200 s<sup>-1</sup> have been measured (Shirley et al., 2006).

The pump–probe method (Sadanaga et al., 2004b) is a second technique proposed for measuring total OH reactivity. Ambient air is sampled into a quasi-static photolysis cell at a flow rate of approximately 10–20 L min<sup>-1</sup>. OH is generated within the reactor from the in situ photolysis of ozone using the emission from a pulsed UV “pump” laser at 266 nm and a frequency of 0.5–10 Hz. OH radicals generated in the photolysis cell react with trace gases from ambient air and time-resolved OH decays are recorded using a FAGE detection. Unlike the TOHLM, in which a steady-state concentration of OH is established for each reaction time (i.e., each position of the injector), the use of a laser to generate OH permits the OH decays to be recorded in real time. This increases the time resolution of the measurement due to the short time needed for OH to react fully (~10–200 ms). In practice, OH decays are averaged over a timescale of 30 s to 5 min to improve the signal-to-noise ratio. An advantage of the pump–probe technique is that ozone photolysis does not generate HO<sub>2</sub>; this reduces potential artifacts from the HO<sub>2</sub> conversion into OH in the presence of ambient NO. Pump–probe instruments exhibit detection limits of 1–4 s<sup>-1</sup> (Table 2), and measurements of ambient OH reactivity up to 120 s<sup>-1</sup> (Lou et al., 2010) have been reported.

The comparative reactivity method (Sinha et al., 2008b) is the most recently developed method for ambient OH reactivity measurements. CRM instruments consist of a small sampling reactor whose operating conditions are varied to monitor competitive reactions of OH with ambient trace gases and a reference compound (pyrrole). Similar to TOHLM, OH is generated by the UV photolysis of water vapor using a mercury lamp, which also leads to the formation of HO<sub>2</sub>. In contrast to the two previous techniques, OH is not directly detected in the CRM instrument. Instead, the loss of OH from reaction with ambient trace gases is derived from a modulation of the pyrrole concentration when zero air and ambient air are successively sampled. The use of a tracer molecule allows for a wider range of detection methods to be used, including mass spectrometry (Sinha et al., 2008b) and gas chromatography (Nölscher et al., 2012b). Compared to laser-based instruments, CRM instruments require smaller flow rates (50–250 cm<sup>3</sup> min<sup>-1</sup>) (Sinha et al., 2008b; Nölscher et al., 2012b), and their design can be simpler and more compact. CRM instruments are sensitive to the secondary formation of OH from HO<sub>2</sub>+NO due to the relatively large HO<sub>2</sub>

concentrations in the CRM reactor, similar to the TOHLM instrument. However, it must be noted that the large concentration of peroxy radicals resulting from pyrrole oxidation competes with HO<sub>2</sub> for the consumption of NO and, to a certain extent, buffers the regeneration of OH in the CRM reactor (Sinha et al., 2008a). In addition, several corrections are required to derive OH reactivity measurements, as described in Sect. 2.2. CRM instruments can easily measure large OH reactivities, as high as 160–300 s<sup>-1</sup>, as reported by Dolgorouky et al. (2012) and Sinha et al. (2008b), but exhibit higher limits of detection than the TOHLM and pump–probe instruments (on average, 3–4 s<sup>-1</sup>; see Table 2). On the other hand, in laser-based instruments, extremely high OH reactivities are more difficult to quantify due to the fast decay of OH radicals inside the reactor.

While the use of OH reactivity instruments during field campaigns has increased, no intercomparison of the three techniques has been reported so far. Given the importance of OH reactivity as a metric of OH chemistry, it is crucial to test the consistency of OH reactivity measurements among techniques to assess their reliability.

The main objective of this work was to compare the CRM and pump–probe techniques in an urban environment exhibiting elevated mixing ratios of NO<sub>x</sub>. As discussed above, measurement artifacts could arise from the reaction of HO<sub>2</sub> with NO in the different instruments, and urban conditions are therefore challenging for ambient OH reactivity measurements. Two instruments, a CRM instrument from Mines Douai and a pump–probe instrument from the University of Lille, were intercompared by sampling urban ambient air and multicomponent standard mixtures. The results presented below are used to evaluate both techniques.

## 2 Experimental

### 2.1 Description of campaign/site

The intercomparison was performed on the campus of the University of Lille in Villeneuve d’Ascq, France, from 9 to 24 October 2012. The sampling location was adjacent to the *Laboratoire de PhysicoChimie des Processus de Combustion et de l’Atmosphère* (PC2A). This site is located in the south-east portion of the Lille metropolitan area and is less than 1 km from several major highways, as shown in Fig. S1 in the Supplement. Due to its location, the site is heavily influenced by anthropogenic emissions of VOCs and NO<sub>x</sub> from vehicular exhaust, residential and light industrial areas, and emissions from laboratory facilities on the university campus.

In addition to the OH reactivity instruments, several analyzers were deployed to measure a comprehensive suite of VOCs and inorganic species. A full listing of supporting measurements is provided in Table 3, and these measurements are described in more detail in Sect. 2.4. Inlets for

**Table 3.** Summary of ancillary measurements used for OH reactivity calculations.

Species	Technique	LOD (ppb) <sup>a</sup> / time resolution (min)	Mixing ratios (ppbv)			Sampling inlet <sup>b</sup>			
			Min.	Max.	Avg. <sup>c</sup>	Outer diameter (mm)	Length (m)	Flow rate (cm <sup>3</sup> min <sup>-1</sup> )	Inlet residence time (s)
54 VOCs:	GC-FID (NMHCs) GC-MS (OVOCs)	0.01–0.06 / 60 0.02–0.09 / 90	12 <sup>d</sup>	1080	33	3.2	10	35	40
14 Alkanes <sup>e</sup> ; 13 Alkenes/Alkynes <sup>e</sup> ; 7 Aromatics <sup>e</sup> ; 22 OVOCs <sup>f</sup>									
NO	Chemiluminescence (Thermo 42i-TLE)	0.05/2	< LOD	290	12 ± 36	6.35	5	2700	1 <sup>g</sup>
NO <sub>2</sub>	Chemiluminescence (Thermo 42i-TLE)	0.1/2	< LOD	56	13 ± 8	6.35	5	2700	1
Ozone	UV absorption (Thermo 49)	0.1/2	< LOD	37	10 ± 9	6.35	5	2700	1

<sup>a</sup> Limit of detection ( $3\sigma$ ); <sup>b</sup> all inlets were made of Teflon; <sup>c</sup> for entire campaign; <sup>d</sup> sum of all VOCs; <sup>e</sup> measured by the NMHC-GC; <sup>f</sup> measured by the OVOC-GC; <sup>g</sup> NO, NO<sub>2</sub>, and Ozone instruments used a common inlet.

all instruments were gathered into a funnel located approximately 50 cm away from the PC2A laboratory building to ensure that all instruments sampled the same air masses.

## 2.2 Description of the Mines Douai CRM (MD-CRM) instrument

### 2.2.1 Technique and instrumentation

As mentioned previously, CRM is a technique based on monitoring competing reactions of OH with a reference compound (pyrrole) and ambient trace gases. Pyrrole was initially chosen as the reference compound for CRM by Sinha et al. (2008b) for several reasons. First, the only known atmospheric source of pyrrole is biomass burning (Karl et al., 2007), and due to its high OH reactivity, ambient concentrations of pyrrole are usually negligible. The rate constant for the reaction of pyrrole with OH ( $1.28 \times 10^{-10} \text{ cm}^3 \text{ molecule}^{-1} \text{ s}^{-1}$ ) (Dillon et al., 2012) has also been well-established and is sufficiently fast to compete with the reactions of other trace gases with OH. Finally, pyrrole can easily be detected by mass spectrometric methods.

A schematic of the MD-CRM instrument is shown as Fig. 1. The instrument consists of a glass reactor that is supplied with various gases (zero air, high purity nitrogen, pyrrole, standard gases) and interfaced to a mass spectrometer, as shown in Fig. 1a. Gas flows are directed through the instrument with solenoid valves (Burkert 6606) and mass flow controllers (MKS 1179A), which are driven by an analog/digital conversion board (National Instruments NI PCI-6024E). The OH reactivity measurements are fully automated and coordinated by a software program written within the LabVIEW environment (National Instruments).

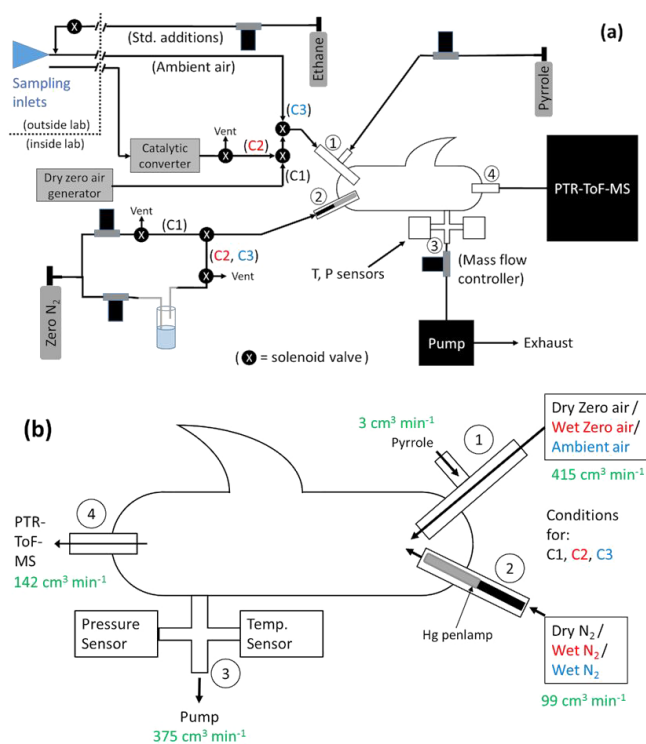
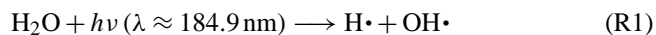


**Figure 1.** Schematic of (a) the entire CRM instrument and (b) the CRM reactor (adapted from Sinha et al., 2008b). In panel (a), gas line connections are indicated by solid black lines. Conditions for the C1, C2, and C3 measurements are represented in both panels by black, red, and blue fonts, respectively. Typical flows through each arm are shown in green fonts adjacent to the respective arms in panel (b).

The glass reactor is based on the design proposed by Sinha et al. (2008b) and features multiple arms (numbered 1 through 4 in Fig. 1b), through which all the required gases are introduced. Approximate flow rates through all four arms are indicated in Fig. 1b. Pressure and temperature within the CRM reactor are recorded by a pressure gauge (MKS Baratron) and a thermocouple attached to arm 3. To produce OH, humidified nitrogen (Praxair, 6.0 purity) is passed through an ultraviolet mercury pen lamp (UVP Pen-Ray, 11sc1) located in arm 2. Water vapor is photolyzed by the 184.9 nm emission of the lamp to produce OH via Reaction (R1).



However, this source of OH also leads to the formation of HO<sub>2</sub>, since H atoms produced in Reaction (R1) can rapidly react with oxygen at the exit of arm 2 via Reaction (R2).



OH can also be produced by the photolysis of ozone in the CRM reactor and the subsequent reaction of excited oxygen atoms with water vapor.

Humid zero air is produced by sampling ambient air through a catalytic converter, which consists of a stainless steel tube (1.27 cm diameter, 20 cm length) filled with 2 g of platinum wool (Shimadzu) and heated to a temperature of 350 °C. The platinum wool leads to the complete oxidation of ambient VOCs to water and carbon dioxide. The zero air humidity is therefore close to ambient relative humidity (RH). The air passes through a 2.6 m of tubing before entering the CRM reactor; this should ensure that the air going through the catalytic converter has been thermalized. While there is the possibility of a slight temperature change between the C2 and C3 conditions (see Sect. 2.2.2), the mercury lamp used to generate OH also releases some heat through arm 1 and tends to buffer the reactor temperature between the C2 and C3 conditions. Measurements of temperature within the CRM reactor (ranging from 24 to 30 °C) suggest that any increase in temperature compared to ambient is lower than 10 °C. Over this range of temperatures, the rate constant for OH + pyrrole differs by less than 5 % based on the temperature-dependent relationship derived by Dillon et al. (2012); this is within the measurement uncertainty for the CRM instrument. The catalytic converter was tested with mixtures made of several tens of hydrocarbons (a few ppbv of each) and was found to efficiently remove VOCs to levels lower than 5–10 pptv (i.e., the detection limits of GC analyzers). During ambient measurements, ambient air is pulled through a 3 m long sampling inlet made of Teflon tubing (0.64 cm o.d.) at a rate of 415 cm<sup>3</sup> min<sup>-1</sup> (Fig. 1b). This air (zero or ambient) is mixed with pyrrole and introduced into the reactor through arm 1. A small flow of a calibration gas (up to 50 cm<sup>3</sup> min<sup>-1</sup> of ethane, 50 ppmv, Praxair) can be added in the sampling line to track the performance of the CRM system during ambient measurements.

A second-generation Proton Transfer Reaction-Time-of-Flight Mass Spectrometer (PTR-ToFMS) (Kore Technology, Ely, UK) samples from the CRM reactor through arm 4. The PTR-ToFMS is used as a detector of pyrrole; the protonated form of pyrrole is detected over an *m/z* range of 68.0 ± 0.4 Dalton. During the intercomparison, the PTR-ToFMS was operated at a reactor temperature of 40 °C and an E / N ratio of 136 Td.

As highlighted by Sinha et al. (2009), the sensitivity of PTR-MS instruments toward pyrrole is dependent on humidity, and the pyrrole signal must be carefully calibrated for relative humidity changes within the CRM reactor. The approach described by de Gouw and Warneke (2007) was employed in this study to account for the effect of water vapor on the PTR-ToFMS sensitivity. This approach involves a normalization of the pyrrole signal to a sum of reagent ion signals (H<sub>3</sub>O<sup>+</sup> + X<sub>R</sub> × H<sub>3</sub>O<sup>+</sup> · H<sub>2</sub>O) that leads to a normalized signal for pyrrole that is independent of humidity. X<sub>R</sub>, a scaling factor for the H<sub>3</sub>O<sup>+</sup> · H<sub>2</sub>O signal, is determined experimentally by measuring the pyrrole signal from a standard mixture under different humidity conditions. For the MD-CRM instrument, X<sub>R</sub> was determined to be 0.6 (Fig. S2).

### 2.2.2 Measurement sequence

The CRM measurement sequence is described in detail by Sinha et al. (2008b) and summarized below. There are three distinct steps in this sequence with the pen lamp on (referred as C1, C2, and C3 below). Another step (C0) is defined as the pyrrole concentration inside the CRM reactor when the mercury pen lamp is off. Each step represents a particular set of operating conditions, which in turn yields a corresponding steady concentration of pyrrole within the reactor (Fig. S3).

During the first (C1) step, pyrrole and dry zero air are introduced into the reactor through arm 1 together with dry nitrogen through arm 2. In the absence of water, OH radicals are not produced, and a baseline C1 concentration is recorded. The relative difference between C0 (lamp off) and C1 (lamp on), i.e. (C0–C1) / C0, is used to estimate the fraction of pyrrole that is lost from direct photolysis inside the reactor, due to photons leaking through arm 2. For the version of the MD-CRM instrument used in this study, approximately 25 % of pyrrole is lost when the lamp is turned on; this is discussed further below.

During a second (C2) step, dry zero air (arm 1) and dry nitrogen (arm 2) are replaced by humid zero air (same RH as in ambient air) and humid nitrogen, respectively. These wet conditions lead to the formation of OH and HO<sub>2</sub> radicals through Reactions (R1) and (R2) as discussed above. Pyrrole reacts with OH, titrating it in milliseconds, which results in the lowering of the pyrrole concentration in the reactor to C2. The difference between C1 and C2 provides information on the amount of OH radicals that react with pyrrole. An apparent pyrrole-to-OH ratio can be calculated from C1 / (C1–

C2). For the MD-CRM instrument, this ratio ranges from 1.5 to 1.8; this is discussed further in Sect. 2.2.3.

During the third (C3) step, humid zero air flowing into arm 1 is replaced by ambient air, keeping the same flow of humid nitrogen in arm 2. Trace gases present in ambient air compete with pyrrole for the available OH radicals. The decrease of pyrrole observed between step 1 and 2 (C1–C2) is offset by the reaction of OH with trace species in the ambient air, and the pyrrole concentration increases from C2 to C3. The magnitude of this increase depends on the amount of OH reactivity in ambient air.

Sinha et al. (2008b) showed that based on pseudo first-order assumptions (i.e., [pyrrole]  $\gg$  [OH]), the total OH reactivity  $k_{\text{OH}}$  can be calculated from measurements of C1, C2, and C3:

$$k_{\text{OH}} = \frac{(C3 - C2)}{(C1 - C3)} k_p C1, \quad (3)$$

where  $k_p$  represents the bimolecular rate constant for the reaction of OH with pyrrole ( $1.28 \times 10^{-10} \text{ cm}^3 \text{ molecule}^{-1} \text{ s}^{-1}$ ) (Dillon et al., 2012).

The measurement scheme used during this study for ambient OH reactivity measurements is described below and summarized in Fig. S3. Measurements of C0 were performed approximately once per day by manually turning off the mercury lamp during the C1 (dry conditions) and C2 or C3 (wet conditions) measurement steps. The measurements of C0 were used to calculate the sensitivity factor of the PTR-MS instrument toward pyrrole (denoted as RF) under humid and dry conditions, as shown in Fig. S4. Measurements of C0 were performed 11 times during the intercomparison period and were used to track the sensitivity of the PTR-MS and the stability of the flow rates over the course of the intercomparison. This figure shows that the stability of the sensitivity was better than 4 %.

C1 was measured every 12 h for a duration of 2 h. As suggested by Sinha et al. (2008b), dry air was used to measure C1 during the intercomparison. The length of this step is necessary to reach the driest conditions possible to minimize residual OH in the reactor, as shown by a plot of the pyrrole signal over time during a C1 measurement (Fig. S5). However, this procedure could result in an underestimation of C1, as it is difficult to remove all trace amounts of water in the reactor. An alternative method to determine C1, which involves the addition of a VOC to scavenge OH in the reactor, has been proposed by Zannoni et al. (2015). The use of this method after this intercomparison study showed that C1 measurements made using dry air in the MD-CRM reactor were higher by about 10 % than those determined using the OH scavenger (Michoud et al., 2015; Zannoni et al., 2015). It is likely that the difference can be attributed to OH radicals produced by photolysis of residual humidity. For this study, the loss of pyrrole under near-dry conditions when the mercury lamp is turned on was determined to be constant (Fig. S9) throughout the campaign at approximately 25 %.

However, this value of 25 % likely represents an upper limit of pyrrole photolysis for this version of the CRM instrument. The impact of an underestimation of C1 on OH reactivity measurements is discussed in Sect. 3.2.1.

After a C1 measurement is completed, C2 and C3 are measured alternately every 2.5 min. The time interval of 2.5 min consists of two subintervals. First, there is 30 s of flushing/equilibration time after a change in the sampling conditions, which ensures that pyrrole has reached a steady concentration in the reactor. After the equilibration is complete, 2 min of pyrrole signal measurements are made at a time resolution of 10 s. An automated calibration test is carried out every 3 h by adding  $50 \text{ cm}^3 \text{ min}^{-1}$  of ethane (50 ppmv, Prax-air) during a C3 measurement. The additional OH reactivity due to the standard addition is determined by subtracting an average value of ambient OH reactivity from the two surrounding measurements made before and after the standard addition. This test is further discussed in Sect. 3.2.1 and allows instrumental performance to be tracked during the campaign.

### 2.2.3 Instrument characterization

Several tests were carried out to characterize the MD-CRM instrument, both in the laboratory before the intercomparison and during the field measurements. These tests are necessary to correct known measurement artifacts associated with the CRM technique and are discussed below.

Sinha et al. (2008b) and Dolgorouky et al. (2012) showed that a variation of humidity between the C2 (wet zero air) and C3 (ambient air) measurements could lead to a change in OH production in the CRM reactor, which in turn could result in a C2 measurement that is not representative of the OH production rate observed during the C3 measurement. For example, as relative humidity increases, the OH concentration increases in the reactor and the pyrrole signal decreases. This artifact is corrected for by first calibrating the C2 sensitivity to humidity and then by correcting C2 to match humidity levels observed during C3.

However, to simplify the derivation of OH reactivity, and to minimize uncertainties, it is desirable to reduce or eliminate the humidity change between C2 and C3. To reduce the humidity correction, ambient air was sampled into a catalytic converter to generate zero air free of VOCs with the same level of humidity as ambient air. Ambient air was first passed through cartridges containing Purafil media (Purafil, Inc.) and activated charcoal located upstream of the catalytic converter to remove  $\text{NO}_x$  species. To test the effectiveness of this setup to remove  $\text{NO}_x$  species, a  $\text{NO}_x$  analyzer was placed at the exit of the Purafil/charcoal trap-catalytic converter system to measure  $\text{NO}_x$  when ambient air was passed through this system. It was found that more than 85 % of ambient  $\text{NO}_x$  was removed. A drawback of this setup was that the adsorption of water onto charcoal altered the relative humidity (RH) of the zero air, leading to a small (up to 10 %)

difference in RH between C2 and C3. Because of this, a correction was still necessary.

Tests were conducted throughout the campaign to investigate the C2 sensitivity to humidity by varying RH in the CRM reactor. The absolute water concentration in the CRM reactor was tracked using the  $m37/m19$  ( $\text{H}_3\text{O}^+ \cdot \text{H}_2\text{O} / \text{H}_3\text{O}^+$ ) ratio calculated from PTR-ToFMS signals. This ratio has been shown to be a suitable metric to track humidity (Inomata et al., 2008) and was found to be proportional to RH for the PTR-ToFMS instrument used in this study. Figure S6 shows that C2 decreases linearly with the  $m37/m19$  ratio for the range of humidity investigated ( $\approx 20$ – $60\%$  RH,  $25^\circ\text{C}$ ). It must be noted that this dependence is not due to the humidity dependence of the PTR-MS sensitivity toward pyrrole, but is only due to a change in OH production in the reactor, as the normalization procedure described in Sect. 2.2.1 was applied to all pyrrole measurements.

The slope of the linear relationship observed between pyrrole concentration and the  $m37/m19$  ratio was used to correct the C2 measurements as shown in Eq. (4).

$$C2_{\text{corr}} = C2_{\text{raw}} + p \left( \left( \frac{m37}{m19} \right)_{C3} - \left( \frac{m37}{m19} \right)_{C2} \right) \quad (4)$$

The value of  $p$  used to correct the C2 measurements ( $C2_{\text{raw}}$ ), calculated as an average of the slopes of the two plots shown in Fig. S6 (made on two different days during the campaign), is  $0.503$  ppbv per percent of change of the  $m37/m19$  ratio.

As discussed previously, ambient NO can generate a measurement artifact due to the formation of OH in the reactor from the reaction of  $\text{HO}_2$  with NO. This artifact affects C3, as ambient NO is introduced into the reactor during this step, leading to an underestimation of the pyrrole concentration, since additional OH reacts with pyrrole. In order to determine the correction for C3, the dependence of the pyrrole signal on NO mixing ratios was investigated at an apparent pyrrole-to-OH ratio of 1.7 using zero air alone and zero air mixed with ethane. The  $\text{HO}_2 + \text{NO}$  artifact was characterized by adding NO at mixing ratios ranging from 5 to 180 ppbv. The decrease in the pyrrole concentration was parameterized as a function of NO, as shown in Fig. S7. This figure shows that the same response is observed for both zero air and zero air + ethane, suggesting that this artifact is independent of ambient OH reactivity. Additional tests performed during laboratory experiments showed that the NO artifact is independent of ambient OH reactivity using compounds other than ethane, including propene and isoprene (Michoud et al., 2015). For NO mixing ratios lower than 50 ppbv, the decrease in C3 is linear with NO and is characterized by a slope  $a_{\text{NO}}$  of  $0.122$  ppbv of pyrrole per ppbv of NO and a zero intercept ( $b_{\text{NO}} = 0$  ppbv of pyrrole). For NO mixing ratios higher than 50 ppbv, a second linear regime is observed, and a different correction is applied using a slope  $a_{\text{NO}}$  of  $0.066$  ppbv of pyrrole per ppbv of NO and an intercept  $b_{\text{NO}}$

of  $4.51$  ppbv of pyrrole. Similar correction curves were determined for another CRM instrument deployed during the MEGAPOLI field campaign (Dolgorouky et al., 2012). This correction was recently investigated through computer modeling for the MD-CRM instrument and was found to be consistent with our understanding of the CRM chemistry (Michoud et al., 2015). The correction applied on C3 for the impact of NO is calculated using Eq. (5).

$$C3_{\text{corr}} = C3 + a_{\text{NO}}[\text{NO}] + b_{\text{NO}} \quad (5)$$

In addition to the correction for NO, it was observed that an addition of  $\text{NO}_2$  into the reactor also leads to a further decrease of the pyrrole signal. This behavior is due to the conversion of  $\text{NO}_2$  to NO from heterogeneous reactions on surfaces such as stainless steel and photolysis (caused by leakage of photons from the mercury lamp inside the reactor). It must be noted that the degree of conversion of  $\text{NO}_2$  to NO within the reactor is sensitive to the position of the lamp within the reactor. Because of this, the conversion of  $\text{NO}_2$  to NO should be characterized for each instrument. The change in the pyrrole signal observed when  $\text{NO}_2$  is added in the CRM reactor suggests that approximately  $46\%$  of  $\text{NO}_2$  is converted into NO. A procedure similar to that described for NO above was applied to correct C3 for this additional  $\text{NO}_2$ .

A third correction must be applied to account for a deviation from first-order conditions as discussed by Sinha et al. (2008b). The derivation of total OH reactivity via Eq. (3) assumes that  $[\text{pyrrole}] \gg [\text{OH}]$  (i.e., pseudo first-order conditions). However, this assumption is not fulfilled within most CRM instruments, as the concentration ratio of pyrrole to OH is usually maintained at a value lower than 2 to enhance the C2–C3 modulation, which in turn improves the detection limit. To correct the CRM measurements for a deviation from pseudo first-order conditions, different concentrations of standards were added inside the reactor to derive a relationship between the CRM measurement and the OH reactivity added in the reactor (Fig. 2). We found that by running the reactor with an apparent pyrrole-to-OH ratio of 1.7, the measured OH reactivity values agree to within  $10\%$  of the OH reactivity expected from the addition of a standard in zero air under both laboratory and field conditions. Furthermore, the correlation between the measured and calculated OH reactivity values seems to be linear, based on the use of three different compounds: ethane ( $k_{\text{C}_3\text{H}_8 + \text{OH}} = 2.4 \times 10^{-13} \text{ cm}^3 \text{ molecule}^{-1} \text{ s}^{-1}$  at  $298 \text{ K}$ ) (Atkinson et al., 2006), ethene ( $k_{\text{C}_2\text{H}_4 + \text{OH}} = 7.9 \times 10^{-12} \text{ cm}^3 \text{ molecule}^{-1} \text{ s}^{-1}$  at  $298 \text{ K}$  and  $1 \text{ bar}$  pressure) (Atkinson et al., 2006), and propene ( $k_{\text{C}_3\text{H}_6 + \text{OH}} = 2.9 \times 10^{-11} \text{ cm}^3 \text{ molecule}^{-1} \text{ s}^{-1}$  at  $298 \text{ K}$  and  $1 \text{ bar}$  pressure) (Atkinson et al., 2006). The OH rate constants of these compounds span 2 orders of magnitude and are representative of reactive gases found in the atmosphere. The agreement observed in Fig. 2 indicates that the CRM instrument accurately quantifies the OH reactivity. Michoud et al. (2015) provide a detailed characterization

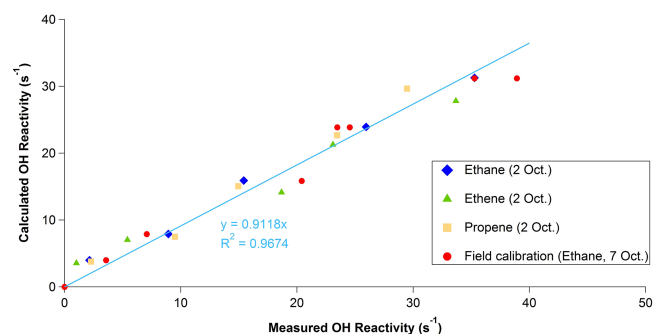


**Figure 2.** Experimental investigation of the deviation from pseudo first-order kinetics for the MD-CRM measurements. Laboratory (2 October) and field (7 October) additions of standard gases are shown on this figure. Ambient measurements must be multiplied by 0.91 when the CRM instrument is run at an effective pyrrole-to-OH ratio of 1.7.

of the MD-CRM instrument and show that experimental determinations of this correction agree relatively well with a modeling of the CRM chemistry.

OH reactivity values calculated from Eq. (3), following the C2 and C3 corrections, were multiplied by 0.912 (the slope of Fig. 2) to derive the OH reactivity in the CRM reactor and to take into account the deviation from first-order conditions for an apparent pyrrole-to-OH ratio of 1.7. During ambient measurements, the apparent pyrrole-to-OH ratio changed from 1.5 to 1.8 due to changes in ambient humidity that impact the production of OH in the reactor. However, subsequent characterizations by Michoud et al. (2015) have shown that this correction factor does not change significantly over this range of pyrrole-to-OH ratios. OH reactivity values were finally corrected for each measurement by a factor of approximately 1.25 to account for ambient air dilution based on the sampling ( $416 \text{ cm}^3 \text{ min}^{-1}$  from Fig. 1b) and total ( $517 \text{ cm}^3 \text{ min}^{-1}$  from Fig. 1b) flow rates inside the reactor.

In practice, the limit of detection (LOD) is governed by the minimum detectable difference between C2 and C3. The LOD for the CRM instrument was estimated by determining the standard deviation ( $\sigma_{C2}$ ) on groups of five successive C2 measurements. An OH reactivity was calculated for each ambient C2 measurement using the corresponding C1 value and assuming a C3 greater than C2 by  $3\sigma_{C2}$ . From the median of these calculated values, it was determined that the MD-CRM instrument has a  $3\sigma$  LOD of  $3.4 \text{ s}^{-1}$ . This LOD is comparable to those reported for other CRM instruments, which range from 3 to  $6 \text{ s}^{-1}$  (Sinha et al., 2008b, 2010; Dolgorouky et al., 2012; Nölscher et al., 2012b). The measurement precision is discussed in Sect. 3.2.1, based on an assessment of the different corrections that must be applied to ambient measurements.

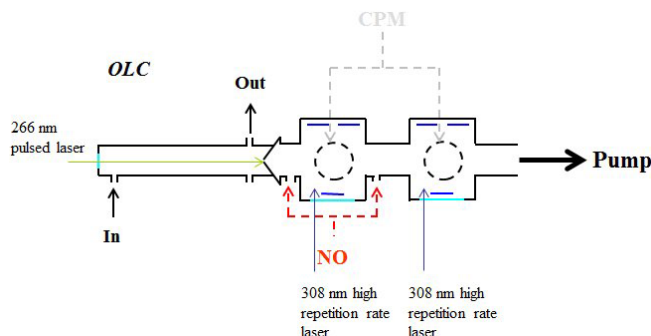


**Figure 3.** Schematic of the UL-FAGE instrument, as configured for OH reactivity measurement.

## 2.3 Description of the University of Lille FAGE (UL-FAGE) pump–probe instrument

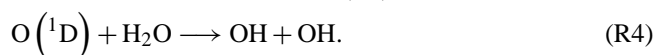
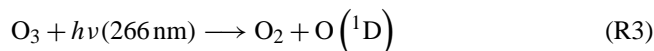
### 2.3.1 Technique and instrumentation

The UL-FAGE instrument can be used in a quantification mode to measure ambient concentrations of OH and  $\text{HO}_2$  radicals or in an OH reactivity mode using the pump–probe method described by Sadanaga et al. (2004). For the latter, the FAGE instrument is coupled to a photolysis cell (Fig. 3), in which a plume of OH is generated by laser photolysis of ozone. Time-resolved OH decays are monitored at a resolution time of  $200 \mu\text{s}$  using the high repetition rate probe laser (5 kHz) of the FAGE instrument. Three other instruments, based on the same technique, are used for field measurements (Sadanaga, 2004b; Lou et al., 2010; Stone et al., 2015). A comparison of the specifications of the different instruments can be found in Table 2.

The UL-FAGE instrument has been described previously (Amedro et al., 2011, 2012; Parker et al., 2011), and only a brief description is given below, focusing on the setup used during this study (i.e., with the FAGE inlet connected at the end of the photolysis reactor, Fig. 3). The photolysis cell is a 50 cm long, 5 cm-i.d. cylindrical tube made of aluminum. A Suprasil quartz window is mounted on one side of the cell, and the other side is directly connected to the FAGE nozzle. The pumping from the FAGE instrument ensures that the photolysis cell is continuously flushed with ambient or zero air. Gases are introduced via Swagelok fittings at the quartz window side of the reactor. During the campaign, ambient air was sampled through a 3 m length of 12.8 mm-i.d. Teflon tubing. The pressure in the cell ( $P \sim 930 \text{ mbar}$ ) was lower than atmospheric pressure due to a restriction of the flow through the sampling Teflon line, which was adjusted to  $8.3 \text{ L min}^{-1}$ .

OH is generated inside the cell by ozone photolysis at 266 nm in the presence of water vapor (Reactions R3, R4) using a quadrupled YAG laser (Quantel, YG 981C) operated

at a pulse repetition rate of 1 Hz.



An ozone mixing ratio of at least 60 ppbv is maintained inside the photolysis cell by injecting a small flow rate of  $20 \text{ cm}^3 \text{ min}^{-1}$  (negligible compared to the main flow through the reactor) of concentrated ozone using an ozone generator (Scientech). The pulse repetition rate of 1 Hz represents a good compromise between the reaction time (1 s or less), the time needed for air exchange in the cell (6.6 s), and the acquisition time (sum of 30 acquisitions of 1 s). The energy of the photolysis laser was set to  $20 \text{ mJ pulse}^{-1}$  for a beam diameter of 2.5 cm, which was achieved after expansion through a telescope. This expansion of the beam permits the generation of OH in a cylindrical volume that is larger than the FAGE nozzle (1 mm) in order to probe a more homogeneous volume with respect to the OH concentration, even if the shape of the beam involves a Gaussian distribution. The pulse duration of the photolysis laser is 20 ns (full-width half maximum).

The photolysis cell is coupled with an airtight connection to the FAGE nozzle where OH is measured by LIF (Laser Induced Fluorescence) using the  $\text{Q}_1(3)$  transition ( $A^2\Sigma^+(v=0) - X^2\Pi(v=0)$ ) at 308 nm after gas expansion into a low pressure cell (1.7 mbar). The laser light is generated using a frequency-doubled dye laser (Sirah Laser PrecisionScan PRSC-24-HPR) pumped by the frequency-doubled output of a Nd:YVO<sub>4</sub> laser (Spectra Physics Navigator II YHP40-532QW). The laser power used to probe OH was approximately 2 mW.

UL-FAGE is composed of two consecutive low-pressure cells based on the Penn State instrument design (Faloona et al., 2004), one being used to measure OH and the other one to measure HO<sub>2</sub>. The laser beam is delivered to the OH cell by a set of optical lenses and fibers. Air from the photolysis cell is pumped by a BOC Edwards GX6/100L pump through a 1 mm orifice after gas expansion into the low-pressure cells. The gas expansion makes it possible to freeze chemical reactions and to extend the fluorescence lifetime of OH. The fluorescence signal is measured perpendicular to the excitation beam by a CPM module (Channel Photomultiplier, Perkin Elmer), which detects photons and converts them to TTL pulses. In the OH reactivity mode, only the first cell dedicated to the measurement of OH is used. The pulses generated from the laser-induced fluorescence of OH are counted by an acquisition card (National Instruments) coupled to acquisition software coded in the LabVIEW environment to automate the measurement sequence, to acquire data, and to process the OH reactivity measurements in real time. The data analysis procedure, based on the exponential fit of a defined number of OH decays, is described in Sect. 2.3.3.

### 2.3.2 Measurement sequence

The OH decay observed is a sum of losses due to chemical reactions, diffusion out of the probed volume, and wall reactions. Under ambient conditions, the OH concentration will follow Eq. (6):

$$[\text{OH}] = [\text{OH}]_0 \exp(-(k_{\text{ambient}} + k_{\text{losses}})t), \quad (6)$$

$k_{\text{ambient}}$  and  $k_{\text{losses}}$  represent first-order losses of OH due to gas-phase and non-gas-phase chemical reactions, respectively. In order to determine the ambient reactivity, two steps are required. First, zero air is introduced in the photolysis cell to quantify the losses ( $k_{\text{losses}}$ ) due to physical processes and wall reactions in the absence of gas-phase chemical reactivity. Then, ambient air is pumped through the photolysis cell to measure the sum of the above-mentioned losses and losses due to the ambient OH reactivity ( $k_{\text{ambient}}$ ). The total ambient OH reactivity is the difference between the first order loss rates of OH measured in ambient air ( $k_{\text{ambient}} + k_{\text{losses}}$ ) and in zero air ( $k_{\text{losses}}$ ).

To measure  $k_{\text{losses}}$ , approximately  $8.3 \text{ L min}^{-1}$  of clean air (99.9%, Praxair 3.0) was provided to the photolysis cell, comprising  $6.3 \text{ L min}^{-1}$  of dry zero air and  $2 \text{ L min}^{-1}$  of zero air humidified with high-purity (Milli-Q) water, which provides enough water (approximately 3000 ppmv) for OH generation. The water concentration was measured by a hygrometer (Michell S8000). As mentioned previously, an additional flow of  $20 \text{ mL min}^{-1}$  of dry zero air and ozone is injected into the photolysis cell to maintain a minimum ozone mixing ratio of approximately 60 ppbv in this cell. Care is taken to perform zero measurements at the same working pressure as during ambient measurements. The OH reactivity in zero air was measured once or twice per day and was found to be  $6.6 \pm 1.2 \text{ s}^{-1}$  ( $n = 16$ ) over the campaign. However, the minimum OH reactivity observed during ambient measurements before the zero subtraction was  $4.8 \text{ s}^{-1}$ , which suggests that the measured zero may be biased high due to residual impurities in zero air.

Tests performed using synthetic mixtures of VOCs (see Sect. 3.1) started and ended with humidified zero air (from a zero air generator and a water bubbler filled with HPLC-grade water). OH reactivity measurements performed with this humid zero air led to a  $k_{\text{losses}}$  value of  $5.6 \text{ s}^{-1}$ , most likely due to the higher quality of the zero air used. For this reason, the  $k_{\text{losses}}$  value of  $5.6 \text{ s}^{-1}$  was used as the pump–probe zero reactivity for the entire intercomparison. It should also be mentioned that during later separated measurements, changing the zero air quality for a higher purity (Air liquid, Alpha1 grade: 99.999%) led to a lower  $k_{\text{losses}}$  value of  $4.5 \pm 0.4 \text{ s}^{-1}$ . However, the configuration of the pump–probe instrument (in particular, the laser type and beam shape) was different during the subsequent measurements; thus, the value of  $k_{\text{losses}}$  measured during the campaign (i.e.,  $5.6 \text{ s}^{-1}$ ) has been preferred for the analysis of measurements made during the intercomparison. These results suggest that the

measurements reported for the pump–probe instrument may be biased low by approximately  $1\text{--}2\text{ s}^{-1}$ , due to impurities in zero air, in the water bubbler, and on the Teflon tubing. These observations highlight the difficulty to accurately determine  $k_{\text{losses}}$ .

### 2.3.3 Instrument characterization

As OH is generated by pulse photolysis and is subsequently probed by the FAGE instrument, the OH profile shows a rapid increase followed by a decrease depending on the OH reactivity. Observed decays were multi-exponential, with a first rapid decrease over a few ms, likely due to the fast diffusion of OH within the photolyzed volume before homogenization. This behavior was previously observed for other pump–probe instruments (Sadanaga et al., 2004b; Lou et al., 2010). In order to quantify the OH reactivity, it is therefore necessary to delay the time at which the mono-exponential fit, representative of the chemistry, starts. A discussion on the choice of the mono-exponential fit for derivation of the total OH reactivity is addressed in the following paragraph.

The UL-FAGE instrument is regularly tested using a gas standard, such as carbon monoxide (CO), whose rate constant with OH is well-known (Parker et al., 2011). Monitoring a kinetic parameter allows for the optimization of experimental conditions such as the beam size, the laser power, and the OH decay fitting window. During these tests, CO is introduced in large excess in the cell at different known concentrations. These tests are carried out under  $\text{NO}_x$ -free conditions, and a single exponential decay of the OH signal down to zero is observed after the first few ms. The pseudo first-order rate constants from the measured OH decays are plotted against the CO concentrations; a linear regression of this plot yields the second-order rate constant. The shortest delay between the photolysis pulse and the start of the fit (0.025 s), during which additional physical losses without chemical interest are observed, was determined by comparing the measured and recommended rate constants for the  $\text{CO} + \text{OH}$  reaction (at 298 K and 1 bar), based on a recommended value of  $2.31 \times 10^{-13} \text{ cm}^3 \text{ molecule}^{-1} \text{ s}^{-1}$  (Atkinson et al., 2006).

A delay of 0.025 s leads to a value of  $2.41 \times 10^{-13} \text{ cm}^3 \text{ molecule}^{-1} \text{ s}^{-1}$  for the  $\text{CO} + \text{OH}$  reaction rate constant, determined from OH reactivity values ranging from 10 to  $90 \text{ s}^{-1}$  ( $R^2 = 0.997$ ). This delay has been used during the present study. Varying the delay from 0.025 to 0.07 s leads to a difference of 7 %, which was accounted for in the total uncertainty calculation and considered as the uncertainty due to the choice of the delay. The delay used in this work is higher than the value used in previous studies (0.008 s in Parker et al., 2011) due to differences in the beam shape, the beam expansion, and the alignment. These results stress that a systematic measurement of OH reactivity using a gas standard should be performed before each campaign and ideally during the campaign. For this study, several tests

were carried out using complex synthetic mixtures of known OH reactivity (Sect. 3.1.2).

During ambient measurements, the duration of the exponential fit is adjusted depending on the OH reactivity level.  $k_{\text{OH}}$  is first estimated ( $k_{\text{OH,estimated}}$ ) by fitting the decay on a duration of 0.038 s, starting after the chosen delay. The decay is then fitted a second time on a duration corresponding to 15 times  $k_{\text{OH,estimated}}$ . A background signal (due to noise) is subtracted considering the signal level after this delay. In practice, the decay is fitted after averaging acquisitions from subsequent photolysis laser pulses (in general 30) to get a signal-to-noise ratio higher than 5.

The performance of the UL-FAGE instrument is similar to that of other pump–probe instruments (Table 2). This instrument can measure OH reactivity values up to  $150 \text{ s}^{-1}$ . Operating conditions described above lead to a precision ( $1\sigma$ ) of 8 % at  $20 \text{ s}^{-1}$  (30 s acquisition) and 10 % at  $100 \text{ s}^{-1}$  (1 min acquisition). The accuracy is estimated to be 20 % ( $1\sigma$ ) from the CO tests. The  $3\sigma$  detection limit determined from zero air measurements is  $3.6 \text{ s}^{-1}$ .

The method to generate OH in the pump–probe technique does not lead to  $\text{HO}_2$  formation. However,  $\text{HO}_2$  can be formed during the reaction of ambient trace gases with OH in the photolysis cell. It is observed that the OH signal does not decay to zero, but instead a slowly decaying residual signal is observed even at long reaction times (Fig. 4). This residual OH signal is estimated to be 0.03 %, due to the recycling of OH radicals from the reaction of  $\text{HO}_2$  with NO, and its intensity, generally a few percent of the initial OH concentration, depends on the NO concentration.

The OH decays are analyzed using a mono-exponential fit in this study. In order to estimate the impact of the recycling chemistry mentioned above on the derivation of OH reactivity measurements, detailed modeling has been carried out below for some observed OH decays. To estimate the bias due to the use of a mono-exponential fit, we carried out a comparison of the decay rates resulting from mono- and bi-exponential fits for several OH decays acquired in a range of different  $\text{NO}_x$  concentrations to decay rates derived from model calculations. In Fig. 4 is shown a decay recorded on 23 October at 21:00 LT, a time period characterized by high NO (91 ppbv) and  $\text{NO}_2$  (38 ppbv) mixing ratios; the residual OH signal due to recycling of peroxy radicals with NO is clearly visible on the logarithmic scale. The bi-exponential least square fit captures the slow decay and closely reproduces the experimental data; taking the fast decay as the OH reactivity leads to a value of  $66 \text{ s}^{-1}$  for  $k_{\text{OH}}$ . A fit to a mono-exponential decay, using only a subset of the data (in this example up to 0.25 ms, obtained such as explained above as 15 times a preliminary decay rate deduced from a linear regression of  $\ln(\text{signal}) = f(t)$  in the time window 0.025–0.063 s) leads to a value for  $k_{\text{OH}}$  of  $59 \text{ s}^{-1}$ , i.e. 10 % below the value obtained from the bi-exponential fit.

The same OH decay is shown on the right panel of Fig. 4 together with OH profiles from model calculations. The

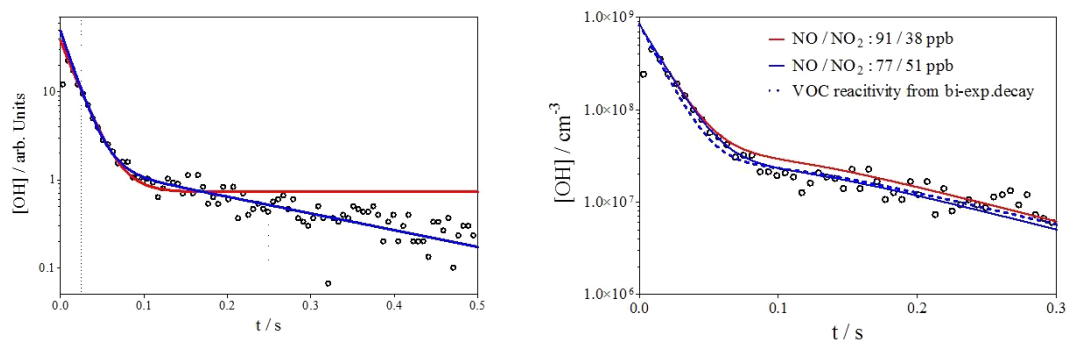


**Figure 4.** Typical OH decay monitored by the UL-FAGE instrument under high  $\text{NO}_x$  conditions. Left panel: mono (red, fitting window: 0.025–0.2 s) and bi-exponential (blue, fitting window: 0.025–0.9 s) fits of the experimental data shown as plain lines. Right panel: comparison of the experimental trace with model simulations (see text and Table S3), VOC concentrations have been adjusted to reproduce the experimental decay. Plain red line: measured NO and  $\text{NO}_2$  mixing ratios. Plain blue line: NO and  $\text{NO}_2$  mixing ratios calculated after addition of  $\text{O}_3$  within the photolysis cell. Dotted blue line: VOC reactivity at the value deduced from the bi-exponential decay.

model used for these calculations is given in the Supplement. OH profiles are shown for two different NO /  $\text{NO}_2$  mixing ratios: the measured ambient mixing ratios (91/38 ppbv), and mixing ratios (77/51 ppbv) calculated based on the conversion of a fraction of NO into  $\text{NO}_2$  due to the addition of 60 ppbv of  $\text{O}_3$  into the photolysis cell and a residence time of 6.6 s. In both cases, the VOC reactivity has been set to best reproduce the measured ambient OH decay. The top trace, simulated using ambient  $\text{NO}_x$  mixing ratios, overpredicts the recycled OH concentration, while experimental data are better reproduced using the NO /  $\text{NO}_2$  partitioning calculated to be present in the cell. Indeed, the addition of high concentrations of  $\text{O}_3$  combined with the rather long residence time before intake into the FAGE cell decreases the impact of NO on the retrieved OH decay.

The first fast decay is mainly due to the reaction of OH with primary species. The second, slow decay is mostly governed by the loss of the recycled OH radicals through reaction of  $\text{RO}_2$  radicals with  $\text{NO}_2$  and to a lesser extent by the reaction of  $\text{HO}_2$  with  $\text{NO}_2$  as well as OH with NO and  $\text{NO}_2$ . Diffusion and wall losses of radicals have very minor contributions. Both modeled traces do not follow a bi-exponential decay, but exhibit a short plateau after the first fast decay before starting the second slower decay. Such a shape reproduces the experimental data very well, as can be seen in particular for the blue trace, but cannot be assimilated to a bi-exponential decay anymore. From the VOC reactivity, used in the model to best reproduce the experimental trace, a  $k_{\text{OH}}$  of  $57 \text{ s}^{-1}$  is obtained, which is closer to the result from the single exponential decay. Using  $k_{\text{OH}}$  such as that obtained from the bi-exponential decay and introducing a corresponding OH reactivity due to reaction with VOC into the model overpredicts the OH decay (dotted blue line in Fig. 4).

Testing this analysis on different traces characteristic of different  $\text{NO}_x$  levels shows that the mono-exponential fit leads to an underestimation only during extreme conditions (30 % at high  $\text{NO}_x$  mixing ratios: 150 ppbv and high

NO /  $\text{NO}_2$ : 2.7), whereas the bi-exponential fit overestimates (by 10–20 %) the reactivity for all the conditions tested by the model ( $\text{NO}_x > 45 \text{ ppbv}$ , NO /  $\text{NO}_2 > 1.2$ ). From these considerations, we have chosen a single exponential decay as the analysis method for this study, even under high  $\text{NO}_x$  concentrations, rather than applying a bi-exponential fit for traces measured under conditions with NO concentrations above a pre-defined threshold, such as proposed by Lou et al. (2010). However, it should be noted that the differences between the mono- and the bi-exponential fits are within the accuracy of the technique. Laboratory experiments are planned in the future to perform a detailed investigation of the impact of this OH recycling on the reactivity measurements.

## 2.4 Measurements of VOCs and ancillary measurements

Ancillary measurements made during the intercomparison are summarized in Table 3. VOC measurements were performed using two online gas chromatographs (GC) from Mines Douai (referred to hereafter as “NMHC-GC” and “OVOC-GC”). These two GCs detected more than 34 NMHCs ( $\text{C}_2$ – $\text{C}_{10}$ ) and 22 OVOCs ( $\text{C}_2$ – $\text{C}_{10}$ ), as reported in Table 3.

The NMHC-GC has been described elsewhere (Badol et al., 2004). Ambient air is sampled through a NAFION membrane and VOCs are trapped at a temperature of  $-30^\circ\text{C}$  inside a quartz tube filled with Carbosieve SIII and Carbopack B. Ambient VOCs are trapped at a sampling flow rate of  $20 \text{ cm}^3 \text{ min}^{-1}$  for a duration of 30 min, leading to a sampling volume of  $600 \text{ cm}^3$ . The trap is located inside a thermodesorption unit (Perkin Elmer, ATD 400) that allows a fast injection of the sample into two columns (PLOT alumine and CPSil 5CB) to separate  $\text{C}_2$ – $\text{C}_6$  and  $\text{C}_6$ – $\text{C}_{10}$  compounds. Two FID detections make it possible to achieve limits of detection of 10–60 pptv at a time resolution of 60 min. NMHCs were measured continuously from 9 to 16 October, but an in-

strumental failure precluded NMHCs measurements from 17 to 23 October.

The OVOC-GC has been described by Roukos et al. (2009). A sampler unit (Markes International, air server Unity 1) allows continuous sampling of ambient air and the trapping of VOCs inside a quartz tube held at 12 °C and filled with Carbo-pack 1B and Carbo-pack X. The sampling flow rate was adjusted to 15 cm<sup>3</sup> min<sup>-1</sup> for a duration of 30 min to sample 450 cm<sup>3</sup> of ambient air. Following the thermodesorption, the GC separation is performed using a high-polarity CP-Lowox column (Varian, France) specially designed for this application. The effect of ambient water on the column separation is minimized by diluting ambient air with dry air (50 : 50) and a trap purge before injection. The identification and quantification of VOCs is performed using a FID/MS coupling. This system exhibits limits of detection in the range 10–90 pptv for a time resolution of 90 min.

Ambient formaldehyde mixing ratios were measured using a pulsed quantum cascade laser mid-infrared ( $\lambda \sim 5.8 \mu\text{m}$ ) absorption spectrometer (Aerodyne Research, Inc.) equipped with thermoelectrically cooled detectors. In this spectrometer, sampled air continuously flows through a low-pressure multipass absorption cell (76 m optical length) installed in the spectrometer housing. Details about the general characteristics and layout of the spectrometer, as well as the principle of operation, can be found in McManus et al. (2010). The thermoelectrically cooled laser is repeatedly swept at high frequency between 1721.6 and 1722.2 cm<sup>-1</sup>. Formaldehyde mixing ratios are derived by fitting the absorption feature using the pressure and temperature measured inside the cell ( $\sim 54.5$  Torr,  $\sim 305$  K) and the HITRAN parameters for formaldehyde (Rothman et al., 2009). Absolute calibration of the instrument is achieved using a 50.6 ppbv sample generated with a permeation device. The 1 min detection limit ( $2\sigma$ ) of the instrument is  $\sim 0.7$  ppbv.

Ambient NO and NO<sub>2</sub> mixing ratios were measured by a commercial analyzer based on chemiluminescence (Thermo 42i Trace Level, LOD: 50 pptv). Ozone was measured by UV absorption (Thermo 49, LOD: 0.1 ppbv) and SO<sub>2</sub> by pulsed UV fluorescence (Thermo 43i, LOD: 0.05 ppbv). Meteorological data (ambient temperature, relative humidity, wind speed and direction, precipitation) was acquired from a meteorological station (Vantage Pro 2, Davis Instruments) located on the roof of a building at a distance of approximately 100 m from the sampling inlet.

CO and methane mixing ratios were not measured during the campaign but are necessary to calculate the total OH reactivity for budgetary analysis. For CO, a constant mixing ratio of 250 ppbv reported as a baseline for Paris by Dolgorouky et al. (2012) was used in this study. However, the measurement site described in Dolgorouky et al. (2012) is considered as a background site, and the CO mixing ratio used may represent a lower limit. A methane background mixing ratio of 1770 ppbv was assumed for this study.

### 3 Results/discussion

#### 3.1 OH reactivity measurements from synthetic VOC mixtures

Two complex standard mixtures of VOCs, one containing 32 NMHCs with mixing ratios of 1–7 ppmv each (Table S1 in the Supplement), and the other containing 29 OVOCs with mixing ratios of 2–3 ppmv each (Table S2), were used to generate diluted mixtures with OH reactivity ranging from 16 to 105 s<sup>-1</sup>. These synthetic mixtures were overflowed into all the sampling inlets. This ensured that the synthetic mixtures were sampled simultaneously by the CRM instrument, the pump–probe instrument, and the two online GC instruments under the same inlet conditions as ambient measurements to investigate the accuracy of the OH reactivity measurements.

##### 3.1.1 MD-CRM instrument

OH reactivity values measured by the CRM instrument were found to be  $(39 \pm 2)\%$  lower than that calculated for the NMHC mixture (Fig. S8b) and  $(53 \pm 0.4)\%$  lower than calculated for the OVOC mixture (Fig. S8a). These values are greater than the  $2\sigma$  uncertainties of 24 and 22 % calculated from a quadratic propagation of uncertainties on the rate constants and the VOC concentration measurements for the NMHC and OVOC mixtures, respectively. Uncertainty calculations were performed assuming that errors on rate constants are independent from each other and that errors on measured VOC concentrations are characterized by an independent random error of 5 % and a similar systematic error of 10 % for each VOC that cannot cancel out through the quadratic propagation of uncertainties on individual OH reactivity values. As discussed below, the OH reactivity measured by the pump–probe instrument for the NMHC mixture, however, agreed well with the calculated OH reactivity values. These results suggest that the MD-CRM instrument underestimates the OH reactivity of complex VOC mixtures, while tests performed using ethane, ethene, and propene did not reveal an underestimation (see Sect. 2.2.3).

These mixtures contain compounds, such as aromatics for NMHCs and acetone for OVOCs, that generally have larger absorption cross-sections at 185 and 254 nm than the calibration gases used to characterize the CRM instrument (ethane, ethene, propene) (Tables S1, S2). Following this study, the MD-CRM instrument was modified to reduce the amount of photons leaking into the reactor (Michoud et al., 2015; Zannoni et al., 2015). The new version of this instrument exhibits less than 5 % of photolysis for pyrrole, compared to approximately 15–25 % in this study. Further tests performed on the modified version of the MD-CRM instrument using mixtures of NMHCs and OVOCs showed a good agreement between the measurements and the OH reactivity expected from these mixtures, with differences lower than 9 % (Michoud et al., 2015). It is therefore likely that the CRM un-

derestimation of the VOC reactivity during this intercomparison experiment was due to photolytic processes inside the reactor, and care must be taken to minimize this issue on CRM instruments, to evaluate these processes, and to ensure agreement between measured and calculated reactivity by performing tests with complex VOC mixtures.

It is interesting to note that if the photolysis of VOCs inside the reactor leads to less reactive species, an underestimation of the OH reactivity is expected. However, the photolysis of VOCs will first lead to the formation of two organic peroxy radicals. If these peroxy radicals quickly react with OH ( $k \approx 10^{-10} \text{ cm}^3 \text{ s}^{-1}$ ), as recently measured for  $\text{CH}_3\text{O}_2$  (Bossolasco et al., 2014) and  $\text{C}_2\text{H}_5\text{O}_2$  (Faragó et al., 2015), an overestimation of the OH reactivity would be expected. This point will need to be investigated further.

### 3.1.2 UL-FAGE instrument

Figure S8 shows a comparison between the measured and calculated OH reactivity values. For NMHCs, the linear regression gives a slope of  $0.99 \pm 0.01$  ( $1\sigma$ ) and a  $R^2$  value of 0.99, indicating a very good agreement between the measured and calculated OH reactivity for this synthetic mixture. These results confirm that the fitting procedure described above is robust and suggest that NMHC photolysis can be neglected.

Due to technical issues, only two measurements were made with the OVOC mixture. A close inspection of Fig. S8 may suggest that UL-FAGE overestimates the OH reactivity by 30 % for the measurement made at a calculated OH reactivity of approximately  $40 \text{ s}^{-1}$ . However, only two measurements are shown on this figure, and more experiments are needed to confirm this observation.

An estimation of the VOC fraction that can be photolyzed by the pump laser can be derived from absorption cross sections at 266 nm and the laser photon density. Benzaldehyde is used as an example, as its absorption cross section at 266 nm ( $2.14 \times 10^{-18} \text{ cm}^2$ ) (Etzkorn et al., 1999) is among the largest for the VOCs present in the OVOC mixture (Table S2). Taking into account the UL-FAGE operating conditions ( $20 \text{ mJ pulse}^{-1}$ ), less than 2.6 % of benzaldehyde is photolyzed per laser shot. If the photolysis of benzaldehyde leads to unreactive species, the OH reactivity from this compound will be decreased. Considering the residence time in the cell and the ratio of the photolyzed volume to the total volume, this would lead to a decrease of 7.8 % ( $0.23 \text{ s}^{-1}$ ). On the other hand, as mentioned above for the CRM instrument, the photolysis of benzaldehyde could produce two  $\text{RO}_2$  radicals, which can then quickly react with OH ( $k \approx 10^{-10} \text{ cm}^3 \text{ s}^{-1}$ ). These conditions correspond to the worst-case scenario, since the rate constant of benzaldehyde with OH is slow ( $1.2 \times 10^{-11} \text{ cm}^3 \text{ s}^{-1}$ ) (Atkinson and Arey, 2003) compared to the reaction of  $\text{CH}_3\text{O}_2$  with OH. The change in the OH reactivity for this compound, considering the OH consumption by  $\text{RO}_2$  (lifetime shorter than 1 s), would be an

increase of approximately 37 %. For 10 ppbv of benzaldehyde, the resultant increase in the OH reactivity would be  $1.2 \text{ s}^{-1}$ , which is within the measurement uncertainty.

If we consider the highest OH reactivity measurements made during these experiments, the same calculation can be done for all NMHCs/OVOCs. The calculations indicate a decrease of  $0.15 \text{ s}^{-1}$  for all NMHCs and  $0.32 \text{ s}^{-1}$  for all OVOCs if the species formed are assumed to be unreactive. If the  $\text{RO}_2$  pathway is considered, this leads to an increase of  $0.5 \text{ s}^{-1}$  for all NMHCs and  $1.17 \text{ s}^{-1}$  for all OVOCs. These results suggest that photolysis of VOCs inside the reactor has a minor impact on the measurements. However, a more complex chemistry may have to be considered if the overestimation of the reactivity is confirmed with OVOC mixtures.

It is interesting to note that if the regression line for the CRM measurements in Fig. S8b (red squares) is not constrained to zero, there is an intercept of  $1.4 \pm 1.0 \text{ s}^{-1}$ . While the uncertainty on the offset is large, this offset would be consistent with an OH reactivity of  $2 \text{ s}^{-1}$  in the zero air. However, it must be noted that any discrepancy in the determination of  $k_{\text{losses}}$  (discussed in Sect. 2.3.2) should not affect the OH reactivity measured by the pump–probe instrument during these tests. This is because the same zero air that was used to measure  $k_{\text{losses}}$  was also used to dilute the standard mixtures. Furthermore, the OH reactivity from the zero air was subtracted from all measurements.

## 3.2 Comparison of ambient OH reactivity measurements

Collocated measurements of ambient OH reactivity with the MD-CRM and UL-FAGE instruments, as described in Sect. 2.1, are discussed below.

### 3.2.1 Performance of the two instruments

For the MD-CRM instrument, C1 was observed to be stable over the course of the 2-week intercomparison with a value of  $47.6 \pm 2.0$  ppbv (Fig. S9), showing a relative standard deviation of approximately 4 %. From measurements of C1 and C0 (as described in Sect. 2.2.2), it was inferred that 25 % of pyrrole is lost when the mercury lamp is turned on. However, as mentioned in Sect. 2.2.2, further testing made after this campaign (Michoud et al., 2015; Zannoni et al., 2015) indicated that this value is an upper limit of the pyrrole fraction that is photolyzed. It is estimated that the pyrrole photolysis was likely lower by 10 % due to residual OH in the reactor during the C1 measurements. However, an underestimation of C1 has opposite effects (though similar in magnitude) on OH reactivity values derived from Eq. (3) and on the correction factor applied for a deviation from first-order kinetics. As a consequence, this error cancels out in the calculation of the corrected OH reactivity measurements, and an increase of C1 by 10 % does not impact the CRM measurements presented in this study.

Field determinations of the correction factor applied to account for a deviation from pseudo first-order kinetics were carried out using ethane at an apparent pyrrole-to-OH ratio of 1.7 and were compared to laboratory results in Fig. 2. A close inspection of this figure shows that the field and laboratory determinations are in good agreement. In order to check the instrument stability, automatic standard additions of ethane were performed every 3 h throughout the campaign (see Sect. 2.2). The concentration of ethane was adjusted to lead to an increase of the OH reactivity by  $24.4 \pm 5.3 \text{ s}^{-1}$ . The average additional OH reactivity from ethane measured for the entire campaign ( $N = 118$  additions) was determined to be  $26.1 \pm 4.0 \text{ s}^{-1}$  (Fig. S10). These results indicate that the CRM instrument ran smoothly during the campaign (i.e., no drift was observed) and also indicate that the OH reactivity from ethane was not significantly impacted by matrix effects.

The impact of the corrections described in Sect. 2.2.3 on the measured OH reactivity values is shown as Fig. S11. The corrections on C2 due to a change of RH between C2 and C3 measurements range from  $-10$  to  $+15 \text{ s}^{-1}$ , with the sign depending on whether humidity was higher or lower during C3 compared to C2. The correction of C3 due to the secondary formation of OH inside the reactor from  $\text{HO}_2 + \text{NO}$  for  $\text{NO}_x$  mixing ratios lower than 40 ppbv (observed most of the time during the first 13 days of the campaign) has a similar impact on the OH reactivity measurements as the humidity correction, with the correction ranging from 0 to  $15 \text{ s}^{-1}$  ( $7.2 \pm 7 \text{ s}^{-1}$  on average). This correction was higher on 22–23 October, when the site experienced unusual elevated  $\text{NO}_x$  mixing ratios of 75–340 ppbv (Figs. 4, S11). These large mixing ratios of  $\text{NO}_x$  led to corrections ranging from 20 to  $110 \text{ s}^{-1}$ , with higher values during the peak of  $\text{NO}_x$  seen on the morning of 23 October.

The correction applied for a deviation from first order conditions is small and is also well characterized. This correction leads to a 10 % decrease of the measured values. The correction applied for dilution leads to an increase of 20 % of the measurements. Overall, while the amplitude of some of the corrections applied on the CRM measurements are large, a good characterization of each correction makes it possible to correct the measurements without introducing unreasonable uncertainties when  $\text{NO}_x$  mixing ratios are lower than 40 ppbv.

The measurement precision ( $1\sigma$ ) derived from measured PTR-MS signals can be computed from  $(\text{LOD}/3) + (5\% \times k_{\text{OH}})$  and is approximately 25, 12, 8, and 7 % at ambient OH reactivity values of 5, 15, 30, and  $60 \text{ s}^{-1}$ , respectively. Based on a quadratic propagation of errors associated with the PTR-MS calibration, the rate constant for the pyrrole + OH reaction, the correction for a deviation from pseudo first-order conditions, and the dilution, the total measurement uncertainty is computed from  $(\text{LOD}/3) + (18\% \times k_{\text{OH}})$  when  $\text{NO}$  mixing ratios are lower than 5 ppbv. The measurement uncertainty is 38, 24, 20, and 19 % for ambient OH reactivity values of 5, 15, 30, and  $60 \text{ s}^{-1}$ , respectively. For  $\text{NO}_x$  mixing

ratios ranging from 5 to 40 ppbv that are associated with ambient OH reactivity values higher than  $10\text{--}20 \text{ s}^{-1}$ , the total uncertainty increases by less than a factor of 1.5 and leads to uncertainty values of 20–30 % (see Michoud et al., 2015 for the methodology used to estimate uncertainties). For  $\text{NO}_x$  mixing ratios higher than 40 ppbv, the total uncertainty increases by up to a factor of 3, leading to total uncertainties in the range 20–70 %.

The UL-FAGE pump–probe instrument ran continuously during the campaign. The pump laser was regularly optimized to maintain an energy of  $20 \text{ mJ pulse}^{-1}$ , which was continuously recorded during ambient measurements using a photodiode. However, it is interesting to note that if a drift in the pulse energy leads to a lower S / N ratio, this will not affect the shape of the decay, keeping the measured OH reactivity unchanged. As mentioned previously, the OH reactivity measured in zero air (99.9 % purity) was stable through the entire campaign ( $N = 16$ ,  $6.6 \pm 1.2 \text{ s}^{-1}$ ) and indicates that instrumental drifts were not significant. The measurement accuracy was tested using CO mixtures at the end of the campaign and was found to be better than 20 % ( $1\sigma$ ). More regular additions of a standard will be performed during future campaigns to track the performances of the UL-FAGE instrument in real-time.

### 3.2.2 Comparison of MD-CRM and UL-FAGE instruments

Figure 5 shows the time series of OH reactivity measurements from the CRM and pump–probe instruments together with mixing ratios of total VOCs and  $\text{NO}_x$ . This figure indicates that measured OH reactivity values were in the range  $5\text{--}100 \text{ s}^{-1}$  with ambient mixing ratios of total VOCs and  $\text{NO}_x$  usually ranging 10–80 and 10–300 ppbv, respectively. Except for the last 3 days of the campaign, where elevated  $\text{NO}_x$  mixing ratios (50–300 ppbv) were observed, these conditions are similar to other urban sites (Dolgorouky et al., 2012; Mao et al., 2010; Shirley et al., 2006).

Diel averages of measurements are shown as Fig. 6. Figure 6a displays average diel profiles of measured reactivity values from both instruments, together with NMHCs, OVOCs and  $\text{NO}_x$  mixing ratios during the weekdays from 8 to 21 October, whereas Fig. 6b shows the same profiles during the weekend. Figure 6c displays the diel averages for 21–23 October, a period that is marked by elevated  $\text{NO}_x$  mixing ratios. Figure 6a–b indicate that two peaks are observed for VOCs and  $\text{NO}_x$  whose timing is consistent with that of peak vehicle traffic (08:30–14:00 and 16:30–21:00), with lower values of OH reactivity and less pronounced peaks on weekends. These peaks are commonly seen in urban environments (e.g., Shirley et al., 2006; Mao et al., 2010; Dolgorouky et al., 2012).

Figures 5 and 6 show that the agreement between the pump–probe and CRM measurements is good from 9 October to 21 October, when ambient  $\text{NO}_x$  mixing ratios are

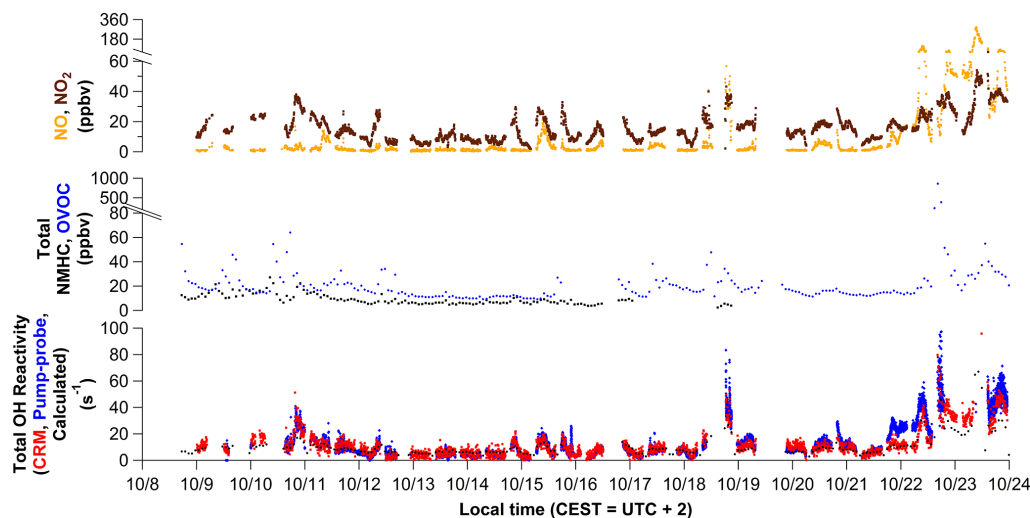


**Figure 5.** Time series of ambient OH reactivity measurements from the CRM (red points) and the pump–probe (blue points) instruments. OH reactivity values calculated from collocated VOC and  $\text{NO}_x$  measurements are also shown (black points). Note the split axes for the  $\text{NO}_x$  (top panel) and OVOC (center panel) traces.

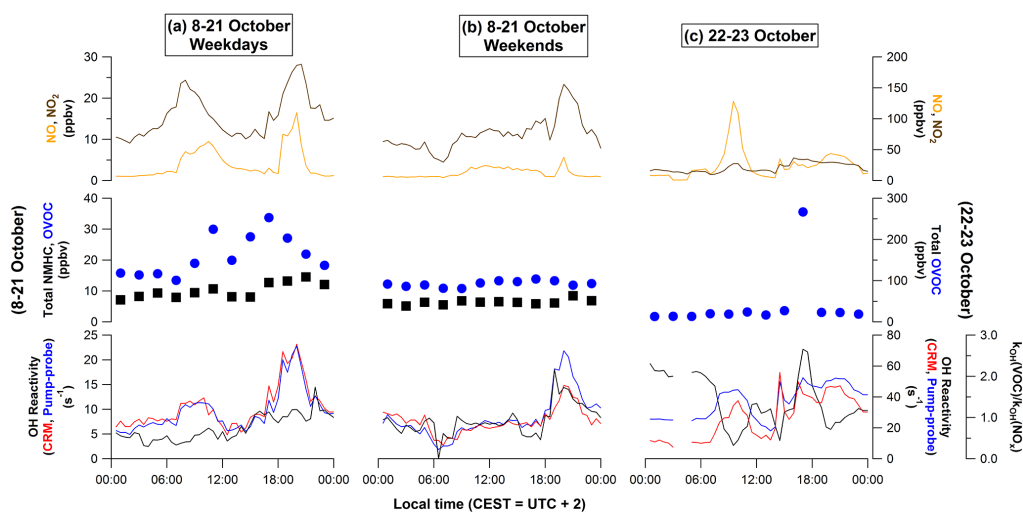


**Figure 6.** Diel averages of  $\text{NO}$  and  $\text{NO}_2$  mixing ratios (top panels), and total NHMC and OVOC mixing ratios (middle panels). Measured OH reactivity values (bottom panels) for (a) weekdays from 8 to 21 October, (b) weekends from 8 to 21 October, and (c) from 22 to 23 October are shown as lines. Note that the scale for (a) and (b) is displayed on the left y axes, and the scale for (c) is displayed on the right y axes. The averaging period for all data is 30 min, except for NMHC and OVOC mixing ratios, which are averaged over a period of 90 min. Also note the absence of NMHC data for 22–23 October due to a failure of one of the GC instruments (see text).

lower than 40 ppbv. Similar trends are observed on the two data sets, and any difference is within the measurement uncertainties. The average diel profiles (Fig. 6a, b) indicate a good agreement for low OH reactivity values when both VOCs and  $\text{NO}_x$  are low and during traffic hours on weekdays, when OH reactivity values up to 20–24  $\text{s}^{-1}$  were measured. In contrast, the agreement is not as good during traffic hours on weekends, which is mainly due to lower CRM measurements recorded on Sunday 21 October 2012 from 19:00

to 24:00. However, this disagreement is within the measurement uncertainties of the two techniques.

At first glance, the relatively good agreement between the two instruments seems to be inconsistent with an underestimation of the total ambient OH reactivity by the CRM instrument due to the photolysis of VOCs inside the sampling reactor as discussed in Sect. 3.2.1. However, a concomitant underestimation of the pump–probe measurements by 2  $\text{s}^{-1}$ , due to a zeroing issue as discussed in Sects. 2.3.2 and 3.1.2, may lead to a fortuitous good agreement. For in-

stance, increasing the pump–probe measurement by  $2 \text{ s}^{-1}$  at a measured OH reactivity of  $10 \text{ s}^{-1}$  would lead to a relative difference of 20%. Assuming that the CRM instrument underestimates the OH reactivity due to VOCs by 45% and taking into account that VOCs and  $\text{NO}_x$  exhibit similar contributions to the total OH reactivity (bottom panels of Fig. 6, black trace), an underestimation of approximately 23% would be expected for the CRM measurements, which is consistent with the underestimation that would be observed if the pump–probe measurements were increased by  $2 \text{ s}^{-1}$ . Due to the nature of the underestimation for each instrument, the effects on the OH reactivity measurements are not apparent in Figs. 5 and 6. While the underestimation by the pump–probe instrument is essentially constant, the underestimation by the CRM instrument varies with the measured ambient OH reactivity.

For  $\text{NO}_x$  mixing ratios greater than 40 ppbv (22–23 October), the agreement between the CRM and pump–probe measurements is still reasonable (Fig. 5), with values for the CRM instrument that are lower by 30% on average than those from the pump–probe instrument, mainly due to the large difference observed on the morning of 22 October. It is interesting to note that the correction procedure used for the CRM measurements seems to be accurate although large corrections are applied.

Figure 7 shows scatter plots of the OH reactivity measured by the CRM and the pump–probe instruments for the whole campaign. The time period from 19:00 LT on 21 October to 07:30 LT on 22 October was not included in the scatter plot and is shown using a different color and symbol. A large difference was observed between the two instruments during this time period, but no obvious reasons were found for this disagreement. A linear regression gives a slope of  $0.78 \pm 0.01$  ( $1\sigma$ ) and an intercept of  $2.16 \pm 0.1$  ( $1\sigma$ )  $\text{s}^{-1}$ , consistent with an underestimation of the OH reactivity by the CRM instrument due to VOC photolysis in the sampling reactor and a bias of approximately  $2 \text{ s}^{-1}$  in the determination of  $k_{\text{losses}}$  for the pump–probe instrument. Since the bias in  $k_{\text{losses}}$  for the pump–probe instrument is independent of the measured ambient OH reactivity, this bias will be reflected in the intercept. Similarly, as the underestimation of OH reactivity by the CRM instrument is relative to the measured OH reactivity, this underestimation will be reflected in the slope. Including the 21–22 October time period in the scatter plot leads to the same slope and an intercept of  $2.74 \text{ s}^{-1}$ . This linear relationship indicates that for ambient OH reactivity values lower than  $10 \text{ s}^{-1}$ , the CRM measurements will be higher than the FAGE measurements, while the opposite is expected for higher ambient OH reactivity values.

A color-coding of the OH reactivity measurements shown in Fig. 7 as a function of the ratio of VOC to  $\text{NO}_x$  reactivity also suggests that the CRM measurements are systematically lower than the pump–probe measurements for ambient OH reactivity values lower than  $35 \text{ s}^{-1}$  when the OH reactivity is driven by VOCs. It is interesting to note that a color-coding

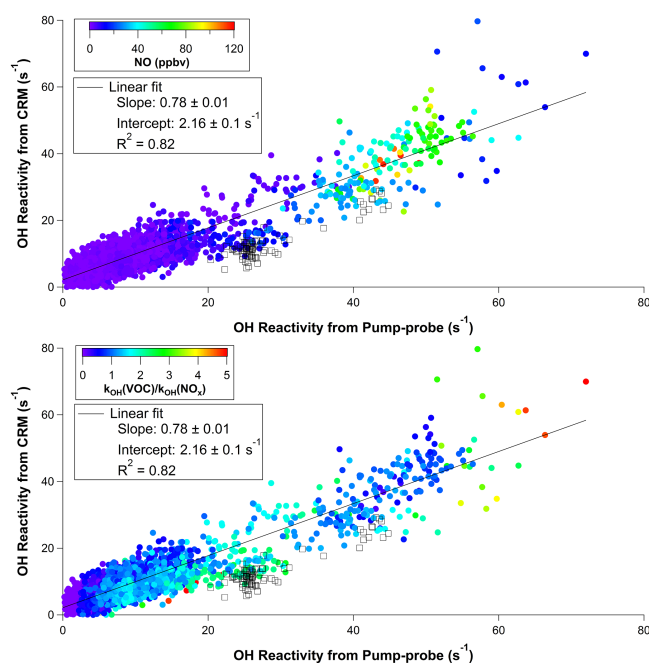


**Figure 7.** Scatter plot of OH reactivity measurements (CRM vs. pump–probe) as a function of  $\text{NO}$  mixing ratios (top) and as a function of the ratio of OH reactivity from VOCs to OH reactivity from  $\text{NO}_x$  (bottom). Black squares show measurements performed from 19:00 LT on 21 October to 07:30 LT on 22 October, when significant differences were observed between the CRM and pump–probe measurements (see text). Note that the pump–probe measurements have been averaged to match the time stamp and the averaging time of the CRM measurements.

as a function of  $\text{NO}$  does not indicate a  $\text{NO}$ -dependent bias and also tends to validate the corrections applied on the CRM measurements.

The results of this intercomparison suggest that some improvements can be made to both instruments. For the pump–probe instrument, a better assessment of the background reactivity is critical to lead to more accurate measurements, especially at low OH reactivity values. High purity water and ultra-high purity air (such as alpha 2 from Air Liquide or, ideally, air produced from liquid  $\text{O}_2$  and  $\text{N}_2$ ) should be used to determine the zero air reactivity.

There are three main areas of improvement for the MD-CRM instrument: (i) a reduction of photolytic processes inside the sampling reactor, (ii) a reduction of the magnitude of the humidity correction, and (iii) a reduction of the magnitude of the  $\text{HO}_2 + \text{NO}$  correction. VOC photolysis can be reduced by modifying the geometry of arm 2 (Fig. 1b) to reduce the amount of photons leaking into the reactor. Reducing the humidity correction requires the use of a generator that can supply zero air free of both VOCs and  $\text{NO}_x$  at a humidity level that mimics ambient air. It is interesting to note that while catalytic converters can be used to generate humid zero air free of VOCs at the same relative humidity than am-

bient air, these converters do not remove  $\text{NO}_x$  species and are not suitable for OH reactivity measurements in urban and suburban areas. The correction to apply for the presence of ambient  $\text{NO}_x$  could be reduced by using a source of OH that does not produce  $\text{HO}_2$ , as the reaction of  $\text{HO}_2$  with NO is the main source of the NO artifact.

After this study, the MD-CRM instrument was optimized to reduce photolysis inside the reactor by changing the position of the mercury lamp. Pyrrole photolysis was decreased to less than 5 % (Michoud et al., 2015; Zannoni et al., 2015), and tests performed with NMHCs (aromatic compounds) and OVOCs (aldehydes, ketones) indicate that less than 1 % of these compounds are photolyzed (Michoud et al., 2015). In addition, further measurements of OH reactivity from complex synthetic mixtures indicated that the new version of the MD-CRM instrument is capable of measuring the OH reactivity of these mixtures at  $\pm 10\%$ . The catalytic converter used during the intercomparison has been replaced by a home-built air generator fed with dry zero air free of both VOCs and  $\text{NO}_x$  and designed to continuously adjust the RH output to match ambient RH. With this air generator, the humidity correction is decreased below  $3\text{--}5\text{ s}^{-1}$  (Michoud et al., 2015).

The reduction of the photon flux inside the reactor also made it possible to reduce  $\text{NO}_2$  photolysis to negligible levels, which in turn makes the MD-CRM instrument less sensitive to the  $\text{HO}_2 + \text{NO}$  artifact. The conversion of  $\text{NO}_2$  into NO decreased from approximately 50–20 %. Work is ongoing to reduce the last 20 % of conversion, which is mainly due to a heterogeneous conversion on surfaces. Tests are also ongoing to determine whether there is a clean source of OH that could be used on the CRM technique to minimize the formation of  $\text{HO}_2$ , and therefore the correction related to ambient NO.

### 3.3 OH reactivity budget

As mentioned in Sect. 2.4, technical issues with one of the GC instruments precluded measurement of the full suite of NMHCs after 16 October. The analysis discussed below, therefore, focuses on the time period where both GC instruments were running (10–16 October).

OH reactivity values were calculated using reaction rate constants calculated at the CRM reactor temperature (25–30 °C) and pressure (985–1000 hPa). While the temperature inside the pump–probe photolysis cell may have been lower by 5–10 °C as the CRM reactor is heated by the mercury lamp, this difference did not impact the intercomparison. Taking into account known temperature dependences for the OH rate constants, values of OH reactivity calculated at a temperature of 20 °C are within 5 % of those calculated at 30 °C.

As mentioned in Sect. 2.4, CO and  $\text{CH}_4$  were not measured during the intercomparison and their mixing ratios were estimated at 250 and 1770 ppbv, respectively. There

were no measurements of ambient formaldehyde mixing ratios from 10 to 16 October. However, measurements were made from 17 to 24 October and are presented as Fig. S12. OH reactivity values were calculated from these measurements in order to estimate the increase in OH reactivity that could be attributed to formaldehyde for the 10–16 October period. The average OH reactivity from formaldehyde was  $1.9 \pm 0.4\text{ s}^{-1}$  from 17 to 21 October and  $2.9 \pm 0.5\text{ s}^{-1}$  from 22 to 24 October.

Figure 8 shows the diel averages of the measured and calculated OH reactivity for 10–16 October.  $\text{NO}_x$  is the dominant source of OH reactivity, with contributions of 40 % around noon and contributions of 50–55 % to the calculated OH reactivity during the peak traffic periods (07:00–09:00 and 18:00–20:00 LT). It is interesting to note that the NO-to- $\text{NO}_2$  conversion discussed for the CRM instrument in Sect. 2.2.3 does not significantly impact the comparison of the measured and calculated OH reactivity values, since the rate constants for OH+NO ( $1.01 \times 10^{-11}\text{ cm}^3\text{ molecule}^{-1}\text{ s}^{-1}$ , 293 K, 760 Torr, IUPAC (<http://iupac.pole-ether.fr/>)) and OH+ $\text{NO}_2$  ( $1.19 \times 10^{-11}\text{ cm}^3\text{ molecule}^{-1}\text{ s}^{-1}$ , 293 K, 760 Torr, IUPAC (<http://iupac.pole-ether.fr/>)) only differ by 15 %. OVOCs, especially ketones and aldehydes, are the next most prevalent sources of OH reactivity and contribute to 15–25 % of the budget. The alkenes make the largest contribution from NMHC species, with  $\text{C}_4$  alkenes being predominant. Alkanes, aromatics and isoprene make minor (< 3 % each) contributions to the OH reactivity.

The calculated OH reactivity is in good agreement with the measurements during both the daytime and nighttime (Fig. 8). It should be noted that  $\text{NO}_x$  chemistry within the reactor is accounted for in the OH reactivity measurements. Measured and calculated OH reactivity values are in agreement within 11 % on average with the CRM instrument and within 37 % on average with the pump–probe instrument, and no significant missing reactivity is observed for this urban environment during the fall period. However, this budget is only based on 1 week of measurements and may not be representative of other time periods. Additional measurements of OH reactivity and VOCs would be necessary to definitively determine whether there is no missing OH reactivity in this environment. It is interesting to note that, in Fig. 8, the OH reactivity values measured by the CRM instrument are higher than those measured by the pump–probe instrument. Indeed, as mentioned in Sect. 3.2.2, this behavior is expected from the linear relationship shown in Fig. 7 for OH reactivity values lower than  $10\text{ s}^{-1}$ .

As shown in Table 1, good agreement between calculated and measured OH reactivity has also been seen in other urban environments. One example is the 2001 PMTACS-NY (PM2.5 Technology Assessment and Characterization Study – New York) field campaign (Ren et al., 2003; Mao et al., 2010), in which the average contribution of  $\text{NO}_x$  to the total OH reactivity is 50 % (Mao et al., 2010). Reasonable

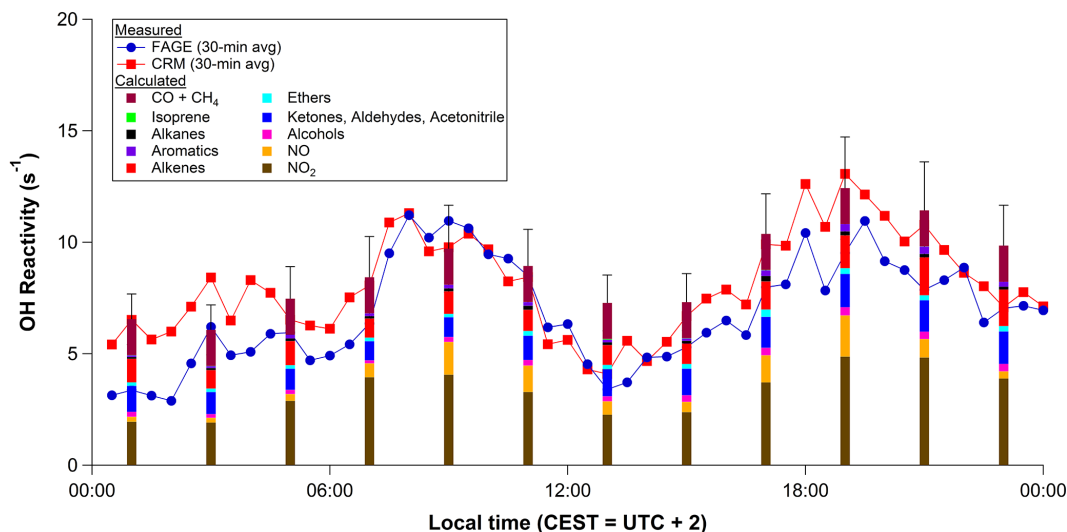


**Figure 8.** Diel averages from 10 to 16 October of the measured (lines and markers, 30 min averages) and calculated (bars, 2 h averages) for the time periods during which OH reactivity, VOCs, and  $\text{NO}_x$  were measured concurrently. Error bars represent  $1\sigma$  uncertainties.

agreement between measured and calculated OH reactivity was also seen in other urban areas within regimes where  $\text{NO}_x$  makes large contributions to the total OH reactivity. This includes a time period dominated by local emissions in Paris (referred to as “period II”) during the MEGAPOLI campaign (Dolgorouky et al., 2012) and winter in Tokyo (Yoshino et al., 2006); during both these time periods,  $\text{NO}_x$  contributed more than 50 % to the total OH reactivity. In addition, agreement between measured and calculated OH reactivity was seen for sites in Houston where OH reactivity was dominated by VOCs, which were generally emitted locally at these sites (Mao et al., 2010). However, missing OH reactivity was observed during spring, summer, and autumn in Tokyo (Yoshino et al., 2006) and for some periods during the MEGAPOLI campaign in Paris (Dolgorouky et al., 2012). It must be noted that the missing OH reactivity observed during these periods was attributed, albeit indirectly, to products of photochemical oxidation of VOCs. As the PC2A site is adjacent to several major highways (Fig. S1) and that this campaign was conducted during autumn, it is likely that primary emissions of  $\text{NO}_x$  and VOCs from vehicle traffic dominate, especially during times of peak traffic.

#### 4 Conclusions

This campaign represents the first successful intercomparison of OH reactivity instruments employing the comparative reactivity method and the pump–probe technique. This intercomparison took place in a  $\text{NO}_x$ -rich environment that is known to be challenging for the CRM technique due to measurement artifacts that are observed when  $\text{NO}$  is present in the sampling reactor. The site was chosen to test the accu-

racy of CRM measurements in  $\text{NO}_x$ -rich environments when important corrections are applied for this artifact.

Both instruments were first tested using mixtures of NMHCs and OVOCs. These tests highlighted that the UL-FAGE pump–probe instrument was accurately measuring the OH reactivity of complex synthetic mixtures made of hydrocarbons. Tests made using a synthetic mixture of OVOCs were inconclusive, and additional work is needed to test the UL-FAGE response to oxygenated compounds. A potential issue linked to the determination of the instrumental zero for the UL-FAGE instrument has been highlighted. Based on measured values of the zero for the pump–probe instrument and the results of linear regressions from ambient and standard measurements, we speculate that this issue could lead to an underestimation of the OH reactivity by up to  $2\text{ s}^{-1}$ . For the MD-CRM instrument, these tests highlighted significant photolysis of VOCs inside the sampling reactor. This issue, if present on other CRM instruments, may lead to an underestimation of the ambient OH reactivity.

The accuracy of the MD-CRM has been tested by comparison to the UL-FAGE instrument during 2 weeks of collocated ambient measurements. A good agreement (slope of 0.78 on a linear correlation plot) was found between the two instruments for ambient  $\text{NO}_x$  mixing ratios as high as 100 ppbv when the appropriate corrections were applied to the CRM measurements. A slope lower than unity seems to be consistent with the photolysis of VOCs inside the CRM sampling reactor, as the tests made using synthetic mixtures led to an underestimation of the OH reactivity.

Following this intercomparison campaign, improvements have been performed on the CRM instrument to reduce photolytic processes within the reactor. As a result, photolysis of VOCs is no longer observed, and the MD-CRM instrument

accurately measures OH reactivity of complex NMHC and OVOC mixtures. The new version of the MD-CRM instrument also incorporates a zero air generator with a dynamic adjustment of humidity to mimic ambient air humidity, reducing the humidity correction.

A comparison of the measured OH reactivity to that calculated from measurements of trace gas concentrations during time periods where the full suite of trace species was available show reasonable agreement. This is consistent with previous measurements in sites where the OH reactivity is dominated by  $\text{NO}_x$  and local VOC emissions.

This work highlights that the use of the CRM technique can be extended to urban and suburban environments if the NO artifact is carefully investigated and well characterized.

**The Supplement related to this article is available online at doi:10.5194/amt-8-4243-2015-supplement.**

*Acknowledgements.* This research was funded by the European Union Seventh Framework Programme under grant agreement 293897 (DEFIVOC project) and the Labex CaPPA. The CaPPA project (Chemical and Physical Properties of the Atmosphere) is funded by the French National Research Agency (ANR) through the PIA (Programme d'Investissement d'Avenir) under contract "ANR-11-LABX-0005-01" and by the Regional Council "Nord-Pas de Calais" and the "European Funds for Regional Economic Development (FEDER)". R. F. Hansen was supported by a Chateaubriand Science Fellowship from the French Embassy of the United States. We thank J. Williams (of MPI Mainz) for providing a spare CRM reactor and the laboratory Laboratoire d'Optique Atmosphérique (LOA) from the University of Lille for providing meteorological data.

Edited by: A. Hofzumahaus

## References

- Amedro, D., Parker, A. E., Schoemaeker, C., and Fittschen, C.: Direct observation of OH radicals after 565 nm multi-photon excitation of  $\text{NO}_2$  in the presence of  $\text{H}_2\text{O}$ , *Chem. Phys. Lett.*, 513, 12–16, doi:10.1016/j.cplett.2011.07.062, 2011.
- Amedro, D., Miyazaki, K., Parker, A., Schoemaeker, C., and Fittschen, C.: Atmospheric and kinetic studies of OH and  $\text{HO}_2$  by the FAGE technique, *J. Environ. Sci.*, 24, 78–86, doi:10.1016/S1001-0742(11)60723-7, 2012.
- Ashmore, M. R.: Assessing the future global impacts of ozone on vegetation, *Plant Cell Environ.*, 28, 949–964, 2005.
- Atkinson, R. and Arey, J.: Atmospheric Degradation of Volatile Organic Compounds, *Chem. Rev.*, 103, 4605–4638, 2003.
- Atkinson, R., Baulch, D. L., Cox, R. A., Crowley, J. N., Hampson, R. F., Hynes, R. G., Jenkin, M. E., Rossi, M. J., Troe, J., and IUPAC Subcommittee: Evaluated kinetic and photochemical data for atmospheric chemistry: Volume II – gas phase reactions of organic species, *Atmos. Chem. Phys.*, 6, 3625–4055, doi:10.5194/acp-6-3625-2006, 2006.
- Badol, C., Borbon, A., Locoge, N., Léonardis, T., and Galloo, J.-C.: An automated monitoring system for VOC ozone precursors in ambient air: development, implementation and data analysis, *Anal. Bioanal. Chem.*, 378, 1815–1824, doi:10.1007/s00216-003-2474-0, 2004.
- Bossolasco, A., Faragó, E. P., Schoemaeker, C., and Fittschen, C.: Rate constant of the reaction between  $\text{CH}_3\text{O}_2$  and OH radicals, *Chem. Phys. Lett.*, 593, 7–13, 2014.
- Chatani, S., Shimo, N., Matsunaga, S., Kajii, Y., Kato, S., Nakashima, Y., Miyazaki, K., Ishii, K., and Ueno, H.: Sensitivity analyses of OH missing sinks over Tokyo metropolitan area in the summer of 2007, *Atmos. Chem. Phys.*, 9, 8975–8986, doi:10.5194/acp-9-8975-2009, 2009.
- de Gouw, J. and Warneke, C.: Measurements of Volatile Organic Compounds in the Earth's Atmosphere Using Proton-Transfer-Reaction Mass Spectrometry, *Mass Spectrom. Rev.*, 26, 223–257, doi:10.1002/mas.20119, 2007.
- Di Carlo, P., Brune, W. H., Martinez, M., Harder, H., Leshner, R., Ren, X., Thornberry, T., Carroll, M. A., Young, V., Shepson, P. B., Riemer, D., Apel, E., and Campbell, C.: Missing OH Reactivity in a Forest: Evidence for Unknown Reactive Biogenic VOCs, *Science*, 304, 722–725, 2004.
- Dillon, T. J., Tucceri, M. E., Dulitz, K., Horowitz, A., Vereecken, L., and Crowley, J. N.: Reaction of Hydroxyl Radicals with  $\text{C}_4\text{H}_5\text{N}$  (Pyrrole): Temperature and Pressure Dependent Rate Coefficients, *J. Phys. Chem. A.*, 116, 6051–6058, doi:10.1021/jp211241x, 2012.
- Dolgorouky, C., Gros, V., Sarda-Esteve, R., Sinha, V., Williams, J., Marchand, N., Sauvage, S., Poulain, L., Sciare, J., and Bonsang, B.: Total OH reactivity measurements in Paris during the 2010 MEGAPOLI winter campaign, *Atmos. Chem. Phys.*, 12, 9593–9612, doi:10.5194/acp-12-9593-2012, 2012.
- Dusanter, S., Vimal, D., Stevens, P. S., Volkamer, R., and Molina, L. T.: Measurements of OH and  $\text{HO}_2$  concentrations during the MCMA-2006 field campaign – Part 1: Deployment of the Indiana University laser-induced fluorescence instrument, *Atmos. Chem. Phys.*, 9, 1665–1685, doi:10.5194/acp-9-1665-2009, 2009.
- Edwards, P. M., Evans, M. J., Furneaux, K. L., Hopkins, J., Ingham, T., Jones, C., Lee, J. D., Lewis, A. C., Moller, S. J., Stone, D., Whalley, L. K., and Heard, D. E.: OH reactivity in a South East Asian tropical rainforest during the Oxidant and Particle Photochemical Processes (OP3) project, *Atmos. Chem. Phys.*, 13, 9497–9514, doi:10.5194/acp-13-9497-2013, 2013.
- Ehhalt, D.: Atmospheric chemistry – radical ideas, *Science*, 279, 1002–1003, 1998.
- Etzkorn, T., Klotz, B., Sørensen, S., Patroescu, I. V., Barnes, I., Becker, K. H., and Platt, U.: Gas-phase absorption cross sections of 24 monocyclic aromatic hydrocarbons in the UV and IR spectral ranges, *Atmos. Environ.*, 33, 525–540, 1999.
- Faloona, I. C., Tan, D., Leshner, R. L., Hazen, N. L., Frame, C. L., Simpas, J. B., Harder, H., Martinez, M., Di Carlo, P., Ren, X., and Brune, W. H.: A Laser-induced Fluorescence Instrument for Detecting Tropospheric OH and  $\text{HO}_2$ : Characteristics and Calibration, *J. Atmos. Chem.*, 47, 139–167, 2004.
- Faragó, E. P., Schoemaeker, C., Viskolcz, B., and Fittschen, C.: Experimental determination of the rate constant of the reaction between  $\text{C}_2\text{H}_5\text{O}_2$  and OH radicals, *Chem. Phys. Lett.*, 619, 196–200, doi:10.1016/j.cplett.2014.11.069, 2015.

- Gryparis, A., Forsberg, B., Katsouyanni, K., Analitis, A., Touloumi, G., Schwartz, J., Samoli, E., Medina, S., Anderson, H. R., Niciu, E. M., Wichmann, H.-E., Kriz, B., Kosnik, M., Skorkovsky, J., Vonk, J. M., and Dörbuda, Z.: Acute effects of Ozone on Mortality from the “Air Pollution and Health: A European Approach” Project, *Am. J. Resp. Crit. Care*, 170, 1080–1087, doi:10.1164/rccm.200403-333OC, 2004.
- Hansen, R. F., Griffith, S. M., Dusanter, S., Rickly, P. S., Stevens, P. S., Bertman, S. B., Carroll, M. A., Erickson, M. H., Flynn, J. H., Grossberg, N., Jobson, B. T., Lefer, B. L., and Wallace, H. W.: Measurements of total hydroxyl radical reactivity during CABINEX 2009 – Part 1: field measurements, *Atmos. Chem. Phys.*, 14, 2923–2937, doi:10.5194/acp-14-2923-2014, 2014.
- Hofzumahaus, A., Rohrer, F., Lu, K., Bohn, B., Brauers, T., Chang, C.-C., Fuchs, H., Holland, F., Kita, K., Kondo, Y., Li, X., Lou, S., Shao, M., Zeng, L., Wahner, A., and Zhang, Y.: Amplified Trace Gas Removal in the Troposphere, *Science*, 324, 1702–1704, doi:10.1126/science.1164566, 2009.
- Ingham, T., Goddard, A., Whalley, L. K., Furneaux, K. L., Edwards, P. M., Seal, C. P., Self, D. E., Johnson, G. P., Read, K. A., Lee, J. D., and Heard, D. E.: A flow-tube based laser-induced fluorescence instrument to measure OH reactivity in the troposphere, *Atmos. Meas. Tech.*, 2, 465–477, doi:10.5194/amt-2-465-2009, 2009.
- Inomata, S., Tanimoto, H., Kameyama, S., Tsunogai, U., Irie, H., Kanaya, Y., and Wang, Z.: Technical Note: Determination of formaldehyde mixing ratios in air with PTR-MS: laboratory experiments and field measurements, *Atmos. Chem. Phys.*, 8, 273–284, doi:10.5194/acp-8-273-2008, 2008.
- Karl, T. G., Christian, T. J., Yokelson, R. J., Artaxo, P., Hao, W. M., and Guenther, A.: The Tropical Forest and Fire Emissions Experiment: method evaluation of volatile organic compound emissions measured by PTR-MS, FTIR, and GC from tropical biomass burning, *Atmos. Chem. Phys.*, 7, 5883–5897, doi:10.5194/acp-7-5883-2007, 2007.
- Kim, S., Guenther, A., Karl, T., and Greenberg, J.: Contributions of primary and secondary biogenic VOC to total OH reactivity during the CABINEX (Community Atmosphere-Biosphere Interactions Experiments)-09 field campaign, *Atmos. Chem. Phys.*, 11, 8613–8623, doi:10.5194/acp-11-8613-2011, 2011.
- Kirchner, F., Jeanneret, F., Clappier, A., Kruger, B., van den Bergh, H., and Calpini, B.: Total VOC reactivity in the planetary boundary layer: 2. A new indicator for determining the sensitivity of the ozone production to VOC and NO<sub>x</sub>, *J. Geophys. Res.*, 106, 3095–3110, doi:10.1029/2000jd900603, 2001.
- Kovacs, T. A. and Brune, W. H.: Total OH Loss Rate Measurement, *J. Atmos. Chem.*, 39, 105–122, 2001.
- Kovacs, T. A., Brune, W. H., Harder, H., Martinez, M., Simpas, J. B., Frost, G. J., Williams, E., Jobson, T., Stroud, C., Young, V., Fried, A., and Wert, B.: Direct measurements of urban OH reactivity during Nashville SOS in summer 1999, *J. Environ. Monitor.*, 5, 2003, 68–74, 2003.
- Kumar, V. and Sinha, V.: VOC-OHM: A new technique for rapid measurements of ambient total OH reactivity and volatile organic compounds using a single proton transfer reaction mass spectrometer, *Int. J. Mass Spectrom.*, 374, 55–63, doi:10.1016/j.ijms.2014.10.012, 2014.
- Lee, J. D., Young, J. C., Read, K. A., Hamilton, J. F., Hopkins, J. R., Lewis, A. C., Bandy, B. J., Davey, J., Edwards, P., Ingham, T., Self, D. E., Smith, S. C., Pilling, M. J., and Heard, D. E.: Measurement and calculation of OH reactivity at a United Kingdom coastal site, *J. Atmos. Chem.*, 64, 53–76, 2009.
- Lou, S., Holland, F., Rohrer, F., Lu, K., Bohn, B., Brauers, T., Chang, C. C., Fuchs, H., Häseler, R., Kita, K., Kondo, Y., Li, X., Shao, M., Zeng, L., Wahner, A., Zhang, Y., Wang, W., and Hofzumahaus, A.: Atmospheric OH reactivities in the Pearl River Delta – China in summer 2006: measurement and model results, *Atmos. Chem. Phys.*, 10, 11243–11260, doi:10.5194/acp-10-11243-2010, 2010.
- Lu, K. D., Rohrer, F., Holland, F., Fuchs, H., Bohn, B., Brauers, T., Chang, C. C., Häseler, R., Hu, M., Kita, K., Kondo, Y., Li, X., Lou, S. R., Nehr, S., Shao, M., Zeng, L. M., Wahner, A., Zhang, Y. H., and Hofzumahaus, A.: Observation and modelling of OH and HO<sub>2</sub> concentrations in the Pearl River Delta 2006: a missing OH source in a VOC rich atmosphere, *Atmos. Chem. Phys.*, 12, 1541–1569, doi:10.5194/acp-12-1541-2012, 2012.
- Lu, K. D., Hofzumahaus, A., Holland, F., Bohn, B., Brauers, T., Fuchs, H., Hu, M., Häseler, R., Kita, K., Kondo, Y., Li, X., Lou, S. R., Oebel, A., Shao, M., Zeng, L. M., Wahner, A., Zhu, T., Zhang, Y. H., and Rohrer, F.: Missing OH source in a suburban environment near Beijing: observed and modelled OH and HO<sub>2</sub> concentrations in summer 2006, *Atmos. Chem. Phys.*, 13, 1057–1080, doi:10.5194/acp-13-1057-2013, 2013.
- Mao, J., Ren, X., Brune, W. H., Olson, J. R., Crawford, J. H., Fried, A., Huey, L. G., Cohen, R. C., Heikes, B., Singh, H. B., Blake, D. R., Sachse, G. W., Diskin, G. S., Hall, S. R., and Shetter, R. E.: Airborne measurement of OH reactivity during INTEX-B, *Atmos. Chem. Phys.*, 9, 163–173, doi:10.5194/acp-9-163-2009, 2009.
- Mao, J., Ren, X., Chen, S., Brune, W. H., Chen, Z., Martinez, M., Harder, H., Lefer, B., Rappenglück, B., Flynn, J., and Leuchner, M.: Atmospheric oxidation capacity in the summer of Houston 2006: Comparison with summer measurements in other metropolitan studies, *Atmos. Environ.*, 44, 4107–4115, 2010.
- Mao, J., Ren, X., Zhang, L., Van Duin, D. M., Cohen, R. C., Park, J.-H., Goldstein, A. H., Paulot, F., Beaver, M. R., Crouse, J. D., Wennberg, P. O., DiGangi, J. P., Henry, S. B., Keutsch, F. N., Park, C., Schade, G. W., Wolfe, G. M., Thornton, J. A., and Brune, W. H.: Insights into hydroxyl measurements and atmospheric oxidation in a California forest, *Atmos. Chem. Phys.*, 12, 8009–8020, doi:10.5194/acp-12-8009-2012, 2012.
- McManus, J. B., Zahniser, M. S., Nelson, D. D., Shorter, J. H., Herndon, S., Wood, E., and Wehr, R.: Application of quantum cascade lasers to high-precision atmospheric trace gas measurements, *Opt. Eng.*, 49, 111124, doi:10.1117/1.3498782, 2010.
- Michoud, V., Hansen, R. F., Locoge, N., Stevens, P. S., and Dusanter, S.: Detailed characterizations of the new Mines Douai comparative reactivity method instrument via laboratory experiments and modeling, *Atmos. Meas. Tech.*, 8, 3537–3553, doi:10.5194/amt-8-3537-2015, 2015.
- Nakashima, Y., Kato, S., Greenberg, J., Harley, P., Karl, T., Turnipseed, A., Apel, E., Guenther, A., Smith, J., and Kajii, Y.: Total OH reactivity measurements in ambient air in a southern Rocky mountain ponderosa pine forest during BEACHON-SRM08 summer campaign, *Atmos. Environ.*, 85, 1–8, doi:10.1016/j.atmosenv.2013.11.042, 2014.
- Nölscher, A. C., Williams, J., Sinha, V., Custer, T., Song, W., Johnson, A. M., Axinte, R., Bozem, H., Fischer, H., Pouvesle, N.,

- Phillips, G., Crowley, J. N., Rantala, P., Rinne, J., Kulmala, M., Gonzales, D., Valverde-Canossa, J., Vogel, A., Hoffmann, T., Ouwersloot, H. G., Vilà-Guerau de Arellano, J., and Lelieveld, J.: Summertime total OH reactivity measurements from boreal forest during HUMPPA-COPEC 2010, *Atmos. Chem. Phys.*, 12, 8257–8270, doi:10.5194/acp-12-8257-2012, 2012a.
- Nölscher, A. C., Sinha, V., Bockisch, S., Klüpfel, T., and Williams, J.: Total OH reactivity measurements using a new fast Gas Chromatographic Photo-Ionization Detector (GC-PID), *Atmos. Meas. Tech.*, 5, 2981–2992, doi:10.5194/amt-5-2981-2012, 2012b.
- Parker, A. E., Amédro, D., Schoemaeker, C., and Fittschen, C.: OH Radical Reactivity Measurements by FAGE, *Environ. Eng. Manag. J.*, 10, 107–114, 2011.
- Pusede, S. E., Gentner, D. R., Wooldridge, P. J., Browne, E. C., Rollins, A. W., Min, K.-E., Russell, A. R., Thomas, J., Zhang, L., Brune, W. H., Henry, S. B., DiGangi, J. P., Keutsch, F. N., Harrold, S. A., Thornton, J. A., Beaver, M. R., St. Clair, J. M., Wennberg, P. O., Sanders, J., Ren, X., VandenBoer, T. C., Markovic, M. Z., Guha, A., Weber, R., Goldstein, A. H., and Cohen, R. C.: On the temperature dependence of organic reactivity, nitrogen oxides, ozone production, and the impact of emission controls in San Joaquin Valley, California, *Atmos. Chem. Phys.*, 14, 3373–3395, doi:10.5194/acp-14-3373-2014, 2014.
- Ren, X., Harder, H., Martinez, M., Leshner, R. L., Oliger, A., Shirley, T., Adams, J., Simpas, J. B., and Brune, W. H.: HO<sub>x</sub> concentrations and OH reactivity observations in New York City during PMTACS-NY2001, *Atmos. Environ.*, 3627–3637, 2003.
- Ren, X., Brune, W. H., Cantrell, C. A., Edwards, G. D., Shirley, T., Metcalf, A. R., and Leshner, R. L.: Hydroxyl and Peroxy Radical Chemistry in a Rural Area of Central Pennsylvania: Observations and Model Comparisons, *J. Atmos. Chem.*, 52, 231–257, 2005.
- Ren, X., Brune, W. H., Mao, J., Mitchell, M. J., Leshner, R. L., Simpas, J. B., Metcalf, A. R., Schwab, J. J., Cai, C., Li, Y., Demerjian, K. L., Felton, H. D., Boynton, G., Adams, A., Perry, J., He, Y., Xhou, X., and Hou, J.: Behavior of OH and HO<sub>2</sub> in the winter atmosphere in New York City, *Atmos. Environ.*, 40, S252–S263, 2006a.
- Ren, X., Brune, W. H., Oliger, A., Metcalf, A. R., Simpas, J. B., Shirley, T., Schwab, J. J., Bai, C., Roychowdhury, U., Li, Y., Cai, C., Demerjian, K. L., He, Y., Zhou, X., Gao, H., and Hou, J.: OH, HO<sub>2</sub>, and OH reactivity during the PMTACS-NY Whiteface Mountain 2002 campaign: Observations and model comparison, *J. Geophys. Res.*, 111, D10S03, doi:10.1029/2005JD006126, 2006b.
- Rothman, L. S., Gordon, I. E., Barbe, I., Benner, D. C., Bernath, P. F., Birk, M., Boudon, V., Brown, L. R., Campargue, A., Champion, J.-P., Chance, K., Coudert, L. H., Dana, V., Devi, V. M., Fally, S., Flaud, J.-M., Gamache, R. R., Goldman, A., Jacquemart, D., Kleiner, I., Lacome, N., Lafferty, W. J., Mandin, J.-Y., Massie, S. T., Mikhailenko, S. N., Miller, C. E., Moazzen-Ahmadi, N., Naumenko, O. V., Nikitin, A. V., Orphal, J., Perevalov, V. I., Perrin, A., Predoi-Cross, A., Rinsland, C. P., Rotger, M., Šimečková, M., Smith, M. A. H., Sung, K., Tashkun, S. A., Tennyson, J., Toth, R. A., Vandaele, A. C., and Vander Auwera, J.: The HITRAN 2008 molecular spectroscopic database, *J. Quant. Spectrosc. Ra.*, 110, 533–572, doi:10.1016/j.jqsrt.2009.02.013, 2009.
- Roukos, J., Plaisance, H., Leonardis, T., Bates, M., and Locoge, N.: Development and validation of an automated monitoring system for oxygenated volatile compounds and nitrile compounds in ambient air, *J. Chromatogr. A*, 1216, 8642–8551, doi:10.1016/j.chroma.2009.10.018, 2009.
- Sadanaga, Y., Yoshino, A., Kato, S., Yoshioka, A., Watanabe, K., Miyakawa, Y., Hayashi, I., Ichikawa, M., Matsumoto, J., Nishiyama, A., Akiyama, N., Kanaya, Y., and Kajii, Y.: The importance of NO<sub>2</sub> and volatile organic compounds in the urban air from the viewpoint of the OH reactivity, *Geophys. Res. Lett.*, 31, L08102, doi:10.1029/2004GL019661, 2004a.
- Sadanaga, Y., Yoshino, A., Watanabe, K., Yoshioka, A., Wakazono, Y., Kanaya, Y., and Kajii, Y.: Development of a Measurement System of OH reactivity in the atmosphere by using a laser-induced pump and probe technique, *Rev. Sci. Instrum.*, 75, 2648–2655, 2004b.
- Shirley, T. R., Brune, W. H., Ren, X., Mao, J., Leshner, R., Cardenas, B., Volkamer, R., Molina, L. T., Molina, M. J., Lamb, B., Velasco, E., Jobson, T., and Alexander, M.: Atmospheric oxidation in the Mexico City Metropolitan Area (MCMA) during April 2003, *Atmos. Chem. Phys.*, 6, 2753–2765, doi:10.5194/acp-6-2753-2006, 2006.
- Sinha, V., Williams, J., Crowley, J. N., and Lelieveld, J.: Technical note: Investigating the influence of NO on the Comparative Reactivity Method, EGU General Assembly, Vienna, Austria, 13–18 April 2008, EGU2008-A-07756, 2008a.
- Sinha, V., Williams, J., Crowley, J. N., and Lelieveld, J.: The Comparative Reactivity Method – a new tool to measure total OH Reactivity in ambient air, *Atmos. Chem. Phys.*, 8, 2213–2227, doi:10.5194/acp-8-2213-2008, 2008b.
- Sinha, V., Custer, T. G., Kluepfel, T., and Williams, J.: The effect of relative humidity on the detection of pyrrole by PTR-MS for OH reactivity measurements, *Int. J. Mass Spectrom.*, 282, 108–111, doi:10.1016/j.ijms.2009.02.019, 2009.
- Sinha, V., Williams, J., Lelieveld, J., Ruuskanen, T. M., Kajos, M. K., Patokoski, J., Hellen, H., Hakola, H., Mogensen, D., Boy, M., Rinne, J., and Kulmala, M.: OH Reactivity Measurements within a Boreal Forest: Evidence for Unknown Reactive Emissions, *Environ. Sci. Technol.*, 44, 6614–6620, 2010.
- Sinha, V., Williams, J., Diesch, J. M., Drewnick, F., Martinez, M., Harder, H., Regelin, E., Kubistin, D., Bozem, H., Hosaynali-Beygi, Z., Fischer, H., Andrés-Hernández, M. D., Kartal, D., Adame, J. A., and Lelieveld, J.: Constraints on instantaneous ozone production rates and regimes during DOMINO derived using in-situ OH reactivity measurements, *Atmos. Chem. Phys.*, 12, 7269–7283, doi:10.5194/acp-12-7269-2012, 2012.
- Stone, D., Whalley, L. K., Ingham, T., Edwards, P. M., Cryer, D., Brumby, C., Seakins, P. W., and Heard, D. E.: Measurement of OH reactivity by laser flash photolysis coupled with laser-induced fluorescence spectroscopy, in preparation, 2015.
- Yoshino, A., Sadanaga, Y., Watanabe, K., Kato, S., Miyakawa, Y., Matsumoto, J., and Kajii, Y.: Measurement of total OH reactivity by laser-induced pump and probe technique – comprehensive observations in the urban atmosphere of Tokyo, *Atmos. Environ.*, 40, 7869–7881, 2006.
- Zannoni, N., Dusanter, S., Gros, V., Sarda Esteve, R., Michoud, V., Sinha, V., Locoge, N., and Bonsang, B.: Intercomparison of two comparative reactivity method instruments in the Mediterranean basin during summer 2013, *Atmos. Meas. Tech.*, 8, 3851–3865, doi:10.5194/amt-8-3851-2015, 2015.